UNIVERSIDAD DE SALAMANCA

SCIENCE FACULTY

BSC IN PHYSICS

BACHELOR'S THESIS

UNRAVELING THE EXOTIC SUPERCONDUCTIVITY IN TWISTED MULTILAYER GRAPHENE

AUTHOR:

GABRIELA ALEJANDRA CHÁVEZ CHÁVEZ

ADVISOR:

DR. MARIO AMADO MONTERO

ACADEMIC YEAR 2022-2023

Desentrañando la superconductividad exótica en grafeno multicapa rotado

Autora: Gabriela Alejandra Chávez Chávez
Tutor: Dr. Mario Amado Montero

Año Académico 2022-2023

Presentado a la Facultad de Ciencias de la Universidad de Salamanca, para la superación de la asignatura Trabajo de Fin de Grado en Físicas en esta Universidad.

Salamanca, a 4 de septiembre de 2023

Fdo.: Gabriela Alejandra Chávez Chávez

Certificado del tutor TFG Grado en Físicas

Dr. Mario Amado Montero, profesor del Departamento de Física Fundamental de la Universidad de Salamanca,

Hace constar:

Que el trabajo titulado "Desentrañando la superconductividad exótica en grafeno multicapa rotado", que se presenta, ha sido realizado por Gabriela Alejandra Chávez Chávez, con NIE Y7462277X y constituye la memoria del trabajo realizado para la superación de la asignatura Trabajo de Fin de Grado en Físicas en esta Universidad.

Salamanca, a 4 de septiembre de 2023

AMADO MONTERO MARIO - DNI 14307293M

Firmado digitalmente por AMADO MONTERO MARIO - DNI 14307293M
Nombre de reconocimiento (DN): c=ES, o=UNIVERSIDAD DE SALAMANCA, ou=CERTIFICADO ELECTRONICO DE EMPLEADO PUBLICO, ou=FACULTAD DE CIENCIAS, ou=1430729302 2002800063, serialNumber=IDCES-14307293M, sn=AMADO MONTERO, givenName=MARIO, cn=AMADO MONTERO MARIO - DNI 14307293M
Fecha: 2023.09.04 19:24:50 +02'00'

Dr. Mario Amado Montero

Abstract

The unprecedented discovery of superconductivity in magic-angle twisted bilayer graphene in 2018 [9] paved the way for the study of moiré systems with more than two layers, and superconductivity has now been found in many of them. In this work, I review the superconductivity of twisted multilayer graphene structures, in particular twisted bilayer and trilayer graphene (TBG and TTG respectively). Starting with the electronic properties of a single graphene layer at low energy, I move on to the Hamiltonian proposed by R. Bistritzer and A. MacDonald (2011) [3] to describe TBG, which can be generalized to a twisted structure with N layers. Irrespective of N, this model predicts a decrease in the Fermi velocity and a series of angles, called "magic angles", at which this velocity vanishes, resulting in a pair of flattened low-energy moiré bands. Once the main theory is settled, I present the evidence confirming these theoretical predictions and study the structures mostly at their largest magic angles, where superconductivity and correlated insulator states have been found when electrostatically doped. The similarity of TBG superconductors to high-temperature superconductors and the possible nature of their superconductivity are explored, and in the case of TTG, I consider the evidence for unconventional superconductivity. Furthermore, the superconductivity observed in twisted tetralayer and pentalayer graphene is briefly studied. I hope that this work can provide an accessible introduction to two-dimensional graphene superconductors and motivate further investigation and discussion.

Keywords: Graphene, superconductivity, twistronics, moiré pattern, correlated insulators

Resumen

El descubrimiento sin precedentes de la superconductividad en el grafeno bicapa rotado de ángulo mágico en 2018 [9] allanó el camino para el estudio de los sistemas moiré con más de dos capas, y ahora se ha encontrado superconductividad en muchos de ellos. En este trabajo, reviso la superconductividad de las estructuras de grafeno multicapa rotado, en particular del grafeno rotado bicapa y tricapa (TBG y TTG, respectivamente). Comenzando con las propiedades electrónicas de una sola capa de grafeno a baja energía, paso al Hamiltoniano propuesto por Bistritzer y MacDonald [3] para describir TBG, el cual puede generalizarse a una estructura rotada con N capas. Independientemente de N, este modelo predice una disminución en la velocidad de Fermi y una serie de ángulos, llamados "ángulos mágicos", en los que esta velocidad desaparece, dando lugar a un par de bandas de moiré aplanadas y de bajas energías. Una vez establecida la teoría principal, presento las pruebas que confirman estas predicciones teóricas y estudio las estructuras especialmente en sus ángulos mágicos mayores, donde se ha encontrado superconductividad y estados aislantes correlacionados cuando se dopan electrostáticamente. Se explora la similitud de los superconductores TBG con los superconductores de alta temperatura y la posible naturaleza de su superconductividad, y en el caso de TTG, considero las pruebas de superconductividad no convencional. Además, se estudia brevemente la superconductividad observada en grafeno rotado de cuatro y cinco capas. Espero que este trabajo pueda proporcionar una introducción accesible a los superconductores bidimensionales de grafeno y motivar nuevas investigaciones y debates.

Palabras clave: Grafeno, superconductividad, twistrónica, patrón moiré, aislantes correlacionados

To my grandma, thank you for building us a home.
To my mom, thank you for giving me your determination and your courage.
To my dad, thank you for encouraging and supporting me to follow my dreams.

Thank you so much, without you I would not be living my dream life.

Contents

1 Introduction **1**

2 Theoretical background **3**

2.1 Introduction to Twisted Multilayer Graphene 3

2.1.1 Unraveling graphene 3

2.1.2 Unraveling Twisted Multilayer Graphene 6

2.2 Mott-like insulators 12

3 Experimental methods **14**

3.1 Experimental techniques used in the research 14

3.2 Sample preparation techniques 15

3.3 Measurements and analysis methods employed 17

4 Results and discussion **19**

4.1 Twisted Bilayer Graphene 19

4.1.1 Experimental results related to superconductivity in MATBG . . . 19

4.1.2 Nematicity 27

4.1.3 Is MATBG a conventional or unconventional superconductor? . . . 27

4.1.4 Possible superconducting mechanism 29

4.2 Twisted Trilayer Graphene 30

4.2.1 Band structure 31

4.2.2 Experimental results related to superconductivity in MATTG . . . 31

4.2.3 Evidence for unconventional superconductivity in MATTG 34

4.3 Twisted Multilayer graphene 36

5 Conclusions **38**

Chapter 1

Introduction

I dare say we have all heard the saying "Unity is strength". For the purposes of this bachelor's thesis, let us modify it as follows: "Unity is strangeness", because elementary particles acting together give rise to fascinating states of quantum matter, such as high-temperature superconductivity and Mott-like insulators, which cannot be the result of their individual contributions. This adage can also be applied to what happens to 2D materials, which exhibit completely different properties when stacked. Graphene, a carbon sheet that is only one atom thick, serves as an illustration of both phenomena. Graphite is metallic, and a single graphene layer is a gapless semiconductor. However, a stack of several layers with alternating twist angles can exhibit a pair of flat bands in the low-energy regime, resulting in a significant correlation between the electrons. Experiments have shown that this leads to superconductivity, correlated insulators, and other quantum states such as a strange metal and a pseudogap phase.

The graphene 'gold rush' [14] began when it was first isolated from graphite in 2004 [25], challenging the idea that it could not exist because strictly 2D crystals were considered to be thermodynamically unstable [21], [30]. The groundbreaking discovery of interaction-induced insulating states and superconductivity in magic-angle twisted bilayer graphene in 2018 [9] paved the way for the study of systems with more than two layers held together by van der Waals forces. These have been shown to be electrically tunable platforms, where the twist angle confers a new degree of freedom that drastically modifies the band diagram and electronic interactions at low energies, opening up a new field called 'twistronics'.

This bibliographical work aims to study and summarize the superconductivity and related phenomena found in various twisted multilayer graphene structures. Personally, I chose the topic because I have been fascinated by superconductivity since high school and by graphene since a friend told me about the discovery of superconductivity in it. I also want to work in the field of condensed matter, in particular by studying quantum materials (especially graphene) and their possible applications, so this topic seemed like a good place to start.

This thesis is structured as follows. Chapter 2 provides a theoretical background, presenting the physics behind twisted bilayer graphene and multilayer structures. In Chapter 3, I describe the experimental and sample preparation techniques and some of the measurements carried out. In Chapter 4, the main findings related to superconductivity in twisted bilayer, trilayer, tetralayer and pentalayer graphene are listed. More emphasis is given to the first two systems, where I also discuss the nature of their superconductivity. Finally, Chapter 5 presents concluding remarks.

Chapter 2

Theoretical background

2.1 Introduction to Twisted Multilayer Graphene

2.1.1 Unraveling graphene

Graphene can be considered a trendy material these days and although it is basically a single, one-atom-thick layer of carbon atoms arranged in a two-dimensional honeycomb lattice, it is stronger than diamond. It was first isolated from bulk graphite around 2004 by A. Geim and K. Novoselov [25], who used Scotch tape to peel off the top layer (see Figure 2.1).

Figure 2.1: Regular Scotch tape used by Andre Geim and Konstantin Novoselov to separate graphene from the graphite bulk on the left, which they donated to the Nobel Prize Museum in Sweden.

In the ground state, a carbon atom has two electrons in the inner shell (level 1) and four electrons in the outermost shell (level 2) which are known as the valence electrons and are the ones that participate in chemical bonding. There is an overlap between the $2s$ orbital and the $2p_x$ and $2p_y$ orbitals that creates three new orbitals, oriented in the graphene plane and separated by 120°. This phenomenon is known as hybridization sp^2 and the electrons in these orbitals form three σ bonds with the nearest carbon atoms in the honeycomb cell. The remaining unhybridized orbital $2p_z$ is perpendicular to the plane

and the delocalized electron in it forms a π bond with the neighborhood carbon atoms. These π-electrons are responsible for the conductivity of graphene. The honeycomb lattice

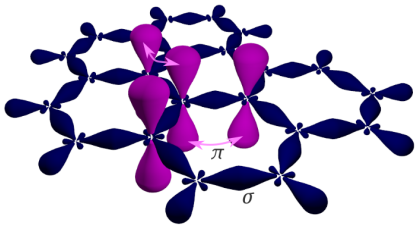

Figure 2.2: σ and π bonds in graphene. Extracted from: Electronic properties of graphene [40] and created by Ponor.

can be seen as a lattice formed by two equivalent atoms A and B where each of them can form a triangular Bravais lattice, so we can choose one of these lattices to be the Bravais lattice of graphene with two atoms A and B as the basis as displayed in Figure 2.3. We

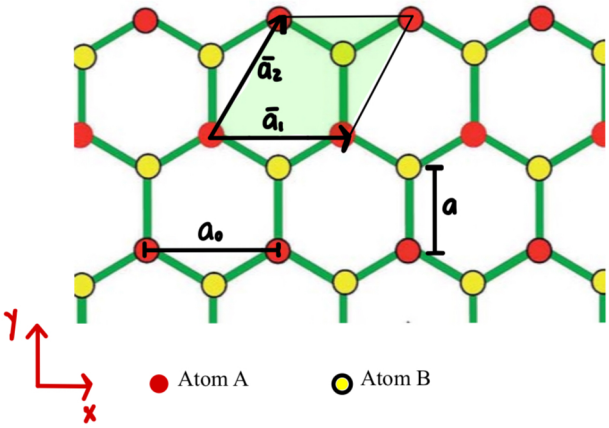

Figure 2.3: The honeycomb lattice of graphene with the triangular Bravais lattice (green area) containing the two atom basis A and B. The vectors $\mathbf{a}_1$ and $\mathbf{a}_2$ are the basis vectors of the lattice. $a = 0.142$nm is the carbon-carbon distance in graphene and $a_0 = \sqrt{3}a$ is the graphene's lattice constant.

can write the position $\mathbf{R}$ of each lattice point forming the graphene Bravais lattice from an arbitrary origin as follows,

$$\mathbf{R}_{n_1,n_2} = n_1\mathbf{a}_1 + n_2\mathbf{a}_2 \qquad n_1,\, n_2 \in Z \tag{2.1}$$

The corresponding reciprocal lattice is defined by

$$\mathbf{G}_{m_1,m_2} = m_1\mathbf{b}_1 + m_2\mathbf{b}_2 \qquad m_1,\, m_2 \in Z \tag{2.2}$$

Moreover, the vectors $\mathbf{a}_i$ and $\mathbf{b}_j$ are related by the relation $\mathbf{a}_i\mathbf{b}_j = 2\pi\delta_{i,j}$. The reciprocal lattice points and the first Brillouin zone are shown in Figure 2.4. The reciprocal lattice is also triangular.

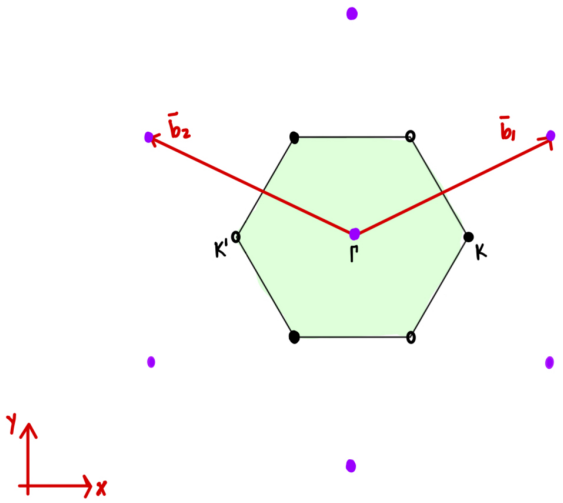

Figure 2.4: The reciprocal lattice points are represented by purple circles. $\mathbf{b}_1$ and $\mathbf{b}_2$ are the basis vectors. The green hexagon is the first Brillouin zone (BZ). K (full circles) and K' (open circles) are special inequivalent points.

To compute the band structure of a single layer of graphene, we consider only the hopping from atom A to the adjacent atom B and vice versa, so that the tight-binding Hamiltonian in the second-quantized form can be written as [10],

$$H = t \sum_{i,j=\langle i \rangle} a_i^\dagger b_j + \text{h.c.} \tag{2.3}$$

where a_i, $a_i^\dagger$ and b_i, $b_i^\dagger$ are the annihilation and creation operators on the A and B atoms respectively and h.c. stands for the Hermitian conjugate. $t \approx -2.7$eV is the nearest hopping energy [10]. If the Hamiltonian is diagonalized, we can obtain the eigenvalues,

$$E_\pm = \pm |f(\mathbf{k})| \tag{2.4}$$

where $\mathbf{k}$ is a vector from the reciprocal space or a wavevector, $f(\mathbf{k}) = \sum_{j=1}^{3} \exp(i\mathbf{k} \cdot \delta_j)$ sums over all three possible hopping paths from B atom to adjacent A atoms (δ_j are the vectors that link the carbon atom B to its three nearest atoms A). The energy dispersion resulting is shown in Figure 2.5 where it can be seen that the two bands touch at the points K and K', which are corners of the first BZ (see Figure 2.4) and are called Dirac points. If the Hamiltonian is expanded in the low energy range, i.e. near one of the two corners (or valleys), for instance K, a massless Dirac Hamiltonian describing a two-level system with inversion symmetry is obtained [10],

$$h_\mathbf{q} = h(\mathbf{K} + \mathbf{q}) \approx \hbar v_F \begin{pmatrix} 0 & q_x - iq_y \\ q_x + iq_y & 0 \end{pmatrix} = \hbar v_F \sigma \cdot \mathbf{q} \tag{2.5}$$

where $\mathbf{q}$ is a small perturbation vector from $\mathbf{K}$, $v_F = 3ta/2\hbar \approx 10^6 \text{m s}^{-1}$ is the effective Fermi velocity[1] and σ are the Pauli matrices. The Dirac points are protected against gap

[1] The Fermi velocity refers to the velocity of electrons near the Fermi level.

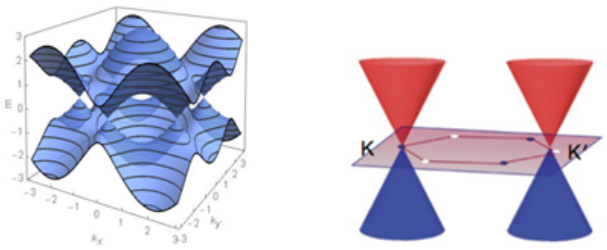

Figure 2.5: **Left**: Energy dispersion or band structure of a single layer of graphene. Extracted from: Study Of Electronic Correlation And Superconductivity In Twisted Graphene Superlattices [10]. **Right**: The low-energy band structure consists of two inequivalent Dirac cones at the Dirac points K and K' of the first BZ (red hexagon). The pink plane is the Fermi surface at charge neutrality and just consists of K and K' points. Extracted from: Graphene bilayers with a twist [1].

opening by a combination of the C_2[2] and T[3] symmetries of the lattice. If the Dirac points were not gapless, their electrons would have a non-zero mass, however, to satisfy both symmetries, their mass must be zero. This explains why graphene is a semimetal. Since the electrons move at a constant speed that is approximately 300 times smaller than the speed of light, they behave as if they were massless ultra-relativistic particles [1]. Finally, K and K' define a valley degree of freedom, which together with spin produces a four-fold band degeneracy [1].

2.1.2 Unraveling Twisted Multilayer Graphene

A moiré pattern is formed when two copies of a periodic pattern are overlaid with a relative twist [3]. In this section, we introduce the electronic properties of Twisted Multilayer Graphene by starting with the simplest system: Twisted Bilayer Graphene.

Twisted Bilayer Graphene (TBG)

The following results are mainly based on references [3] and [1].

A twisted bilayer graphene system (TBG) can be obtained by rotating the second layer by an angle θ (anti-clockwise and about the origin) of a Bernal stacking configuration and finally translating it by a vector τ.

As we have already seen, a single layer of graphene has a linear energy dispersion at low

[2] C_2 is the 2D spatial inversion operator that takes (x, y) to $(-x, -y)$, therefore it demands $m(K) = m(K')$ with m the mass of the Dirac points [10]

[3] T is the time reversal operator, hence it demands $m(K) = -m(K')$ with m the mass of the Dirac points [10].

energies. Here we will see how the electronic band structure in this regime is modified when another graphene sheet is stacked on top of the original and rotated by an angle θ relative to it.

The moiré pattern of TBG (see Figure 2.6) can be seen using scanning tunnelling microscope (STM) and consists of AA and AB/BA regions with a period of $L \approx a_0/(2\sin(\theta/2))$. In the AA regions, each atom in the top layer has a matching atom directly beneath it in the bottom layer. In the AB regions, each A atom in the top layer is right above an atom in the bottom layer, while the B atoms on the top layer do not have a matching atom in the bottom layer, and vice versa for BA regions.

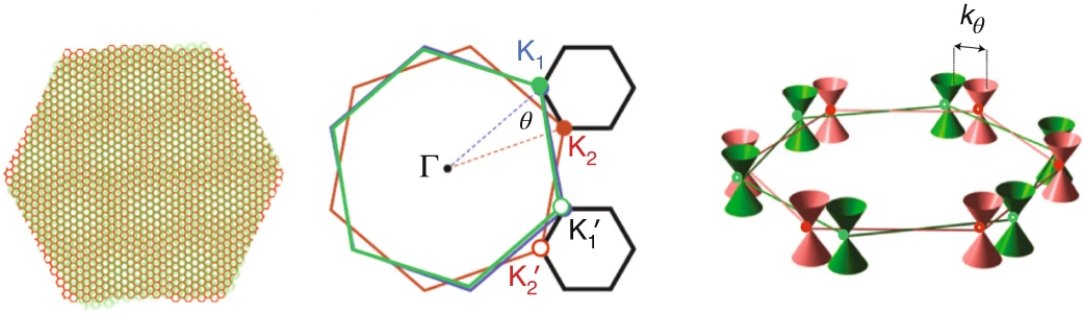

Figure 2.6: **Left**: Moiré pattern of TBG. The bright spots correspond to AA regions and the dark spots to AB or BA regions. **Middle**: Moiré mini-Brillouin zones (black hexagons) resulting from superposing the first Brillouin zones of the top (green) and bottom (red) graphene layers. The sides of the two hexagons are given by $K_1 - K_2$ and $K_1' - K_2'$. **Right**: Dirac cones of the top (green) and bottom (red) graphene layers and the twist-angle dependent displacement, $k_\theta = 2|K|\sin(\theta/2)$. Extracted from: Graphene bilayers with a twist [1].

The shift between the Dirac cones K and K' of the top and bottom layers gives rise to two inequivalent hexagonal mini-Brillouin zones with sides $k_\theta \approx 2K\sin(\theta/2)$, as shown on the right of Figure 2.6. Each mini-Brillouin zone contains two Dirac cones, one from each layer, at its corners. They are also protected by the C_2T symmetry, which can be broken by breaking C_2 or T, leading to the formation of spectral gaps.

Since TBG is not a crystalline structure for most angles, it is necessary to construct a model describing the system that is valid for any value of θ. R. Bistritzer and A. MacDonald (2011) [3] proposed a low-energy continuum model Hamiltonian for the K Dirac points of a TBG that is valid for any $\theta \lesssim 10°$ and τ. It consists of three terms: two that account for the isolated layers and a tunneling term that describes a process in which an electron with momentum $\mathbf{p'} = M\mathbf{p}$ residing on sublattice β in one layer hops to a momentum state $\mathbf{k}$ and sublattice α in the other layer. The first two can be written using the Dirac Hamiltonian for a monolayer (eq. (2.5)) rotated by an angle θ with respect to a fixed coordinate system and for the third one, they derived it by using a π-band tight-binding model to write the wave functions and assuming that the interlayer tunneling amplitude between π orbitals is a smooth function of the spatial separation

projected onto the graphene planes. It turned out that the interlayer tunneling amplitude fell to zero very quickly with the magnitude of the momentum, so only the largest values were taken. This resulted in three distinct hopping processes, each identified by a different three-momentum transfer $\mathbf{q}_j$, which when repeated produce a k-space honeycomb lattice (each hexagon of it is the same as the hexagon representing the mini-Brillouin zone in Figure 2.6), as shown in Fig 2.7.

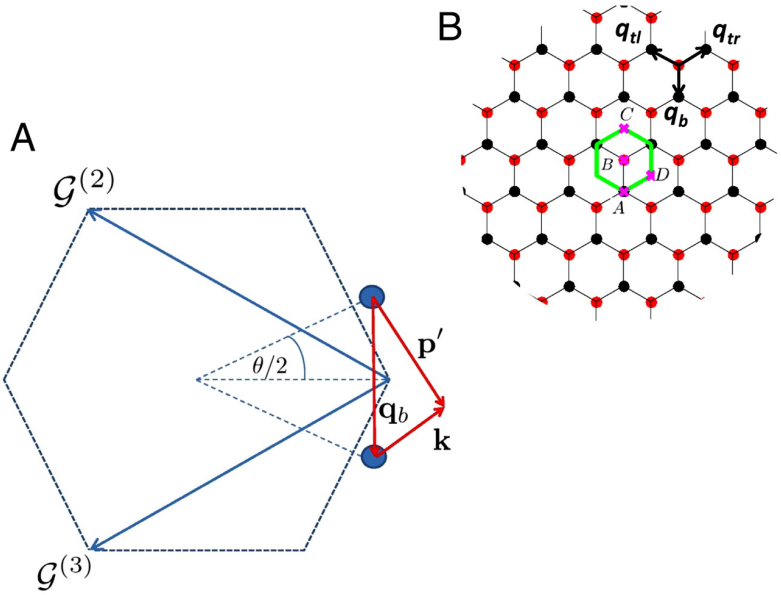

Figure 2.7: **A**: $\mathbf{q}_b$ represents a three momentum transfer of one of the three hopping processes in which an electron with momentum $\mathbf{p'} = M\mathbf{p}$ residing on sublattice β in one layer hops to a momentum state $\mathbf{k}$ and sublattice α in the other layer. **B**: Repeating the hopping processes with wave vectors $\mathbf{q}_j$ generates a k-space honeycomb lattice. For all the three processes $|\mathbf{q}_j| = k_\theta$, however, the hopping directions are $(0, -1)$ for $j = b$, $(\sqrt{3}/2, 1/2)$ for $j = tr$, and $(-\sqrt{3}/2, 1/2)$ for $j = tl$. The red and black circles mark the Dirac points of the two layers and the green hexagon represents the moiré band Wigner-Seitz cell. Extracted from: Moiré bands in twisted double-layer graphene [3].

The continuum model hopping is then local and periodic, allowing Bloch's theorem to be applied at any rotation angle irrespective of whether or not the bilayer is crystalline [3]. With this in hand, the Hamiltonian matrix obtained is roughly $\approx 10\theta^{-2}$ for small θ (in degrees). When the momentum-space lattice is truncated at the mini-BZ and the sublattice degree of freedom is included, the low-energy Hamiltonian of TBG for the K mini-Brillouin zone can be written as follow [3],

$$H_{\mathbf{k}} = \begin{pmatrix} h_{\mathbf{k}}(\theta/2) & T_b & T_{tr} & T_{tl} \\ T_b^\dagger & h_{\mathbf{k}_b}(-\theta/2) & 0 & 0 \\ T_{tr}^\dagger & 0 & h_{\mathbf{k}_{tr}}(-\theta/2) & 0 \\ T_{tl}^\dagger & 0 & 0 & h_{\mathbf{k}_{tl}}(-\theta/2) \end{pmatrix} \tag{2.6}$$

where $\mathbf{k}$ is in the moiré BZ and $\mathbf{k}_j = \mathbf{k} + \mathbf{q}_j$ and T_j are the 2x2 interlayer hopping matrices. The Hamiltonian for the K' mini-Brillouin zone is the time reversal of $H_{\mathbf{k}}$.

Figure 2.8 displays the moiré bands as a function of their min-BZ momentum **k** computed numerically and by truncating momentum space at lattice vectors of the order of $w/\hbar v_F$, where w is the hopping energy.

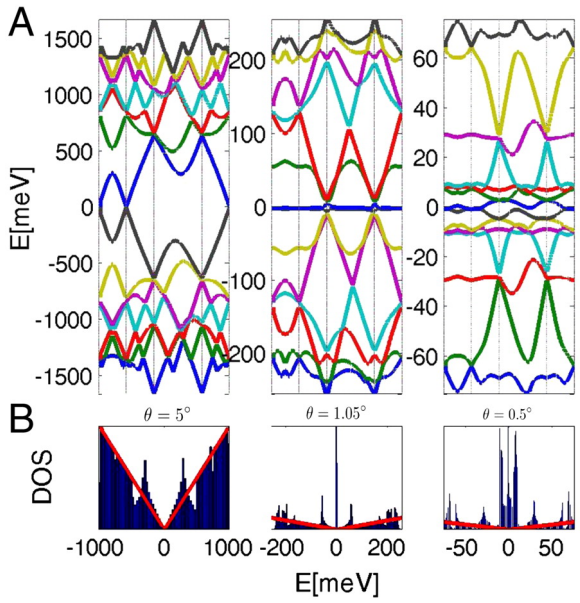

Figure 2.8: **A**, Energy dispersion for the 14 bands closest to the Dirac point for $w = 110$meV and twist angles $\theta = 5°$, $1.05°$ and $0.5°$. **B**, Density of states (DOS). Extracted from: Moiré bands in twisted double-layer graphene.

Before continuing, let us take a look at the degeneracy of bands in TBG with the outstanding help of ref. [10].

Loosely speaking, degeneracy means that two states of different momentum occupy the same energy. If we look at the middle sketch in Figure 2.6, we can see that we can pair K_1 with K_2 and K_1' with K_2' and call them bands of K and K' valleys respectively[4], therefore, it is possible to have a valley degeneracy, because time reversal symmetry guarantees that the bands at opposite valleys satisfy,

$$E_{\mathrm{K}}(\mathbf{q}) = E_{\mathrm{K}'}(-\mathbf{q}) \tag{2.7}$$

If we count the spin, the bands in TBG are four-fold degenerate. This same spin-valley degeneracy is held, regardless of the number of layers, regardless of the number of layers as will be mentioned in 2.1.2.

Van Hove singularities (VHSs) are points of high density of states (DOS) in the band structure and can be identified as peaks in the scanning tunneling spectroscopy (STS) spectrum of the material. In TBG a pair of pronounced VHS peaks flanking a minimum

[4]We could have also made the association, K_1, $K_2' \leftrightarrow K_s$ and K_2, $K_1' \leftrightarrow K_s'$

DOS at the Dirac point, have been observed and as the twist angle is reduced the two VHS peaks move closer together (see Figure 2.9).

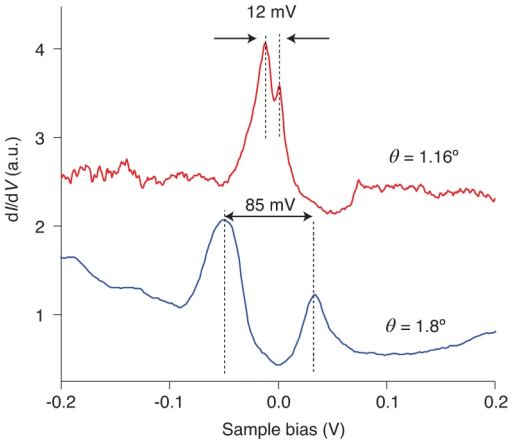

Figure 2.9: STS spectrum at the centre of an AA region of the moiré pattern (i.e. dI/dV vs. voltage sample) at two different twist angles, $\theta = 1.16°$ (red trace) and $\theta = 1.8°$ (blue trace). A minimum at the Dirac point and flanked by two VHS peaks can be seen in both traces. As the twist angle is reduced the two VHS peaks merged into a DOS peak with a small pseudogap at the Dirac point. Extracted from: Graphene bilayers with a twist [1].

In addition to introducing VHSs (which are not seen in the Bernal-stacked bilayer and in a monolayer of graphene), the moiré pattern also lowers the Fermi velocity, $\nu^\star = \partial_{\mathbf{k}} (\epsilon^\star_{\mathbf{k}})_{\mathbf{k}=\mathbf{K}}$ where $\epsilon^\star_{\mathbf{k}}$ represents the eigenvalues of the Hamiltonian describing TBG, to $\nu* = v_F(1-3\alpha^2)/(1+6\alpha^2)$ ($\nu*$ to the lowest order), where $\alpha = w/(\hbar\nu_{\mathrm{F}}\mathrm{k}_\theta)$. This was predicted theoretically [3] and can be confirmed by Landau-level spectroscopy measurements. Furthermore, they found that this velocity at the Dirac-point, has a nonmonotonic dependence on θ at small angles and vanishes at a series of angles called "magic angles": $\theta \approx 1.05°, 0.5°, 0.35°, 0.24°$, and $0.2°$.

In this work, we are interested in the largest magic angle, called the first magic angle, because superconductivity was discovered very close to it ($\theta \approx 1.1°$) [9]. As mentioned above, at this angle, the Dirac point velocity vanishes and is accompanied by a pair of flattened low-energy moiré bands (the lowest conduction band, and the highest valence band), with bandwidth of about 5–10meV [9], which contributes to a DOS peak at the Dirac point discussed before (see Figure 2.9) [3].

As can be seen in Figure 2.8 for $\theta = 1.05°$, the flat bands are separated from other bands by single-particle gaps (also known as superlattice gaps).

Since the electrons are localized in the flat bands (due to the DOS peak at the Dirac point), the formation of correlated insulators is not the only phenomenon seen, as strong interactions (due to localization) can also give rise to superconductivity, magnetism, charge density waves, quasiparticles with exotic statistics, and other phenomena [24].

Twisted Multilayer Graphene

The following results are mainly based on reference [27].

The discovery of superconductivity in magic-angle TBG (MATBG) in 2018 [9], paved the way for the study of moiré systems with more than two layers, and superconductivity has now been found in many structures at their respective magic angles, namely magic angle twisted trilayer [28], [15], [19], tetralayer, pentalayer graphene (MATTG, MAT4G and MAT5G respectively) and twisted double bilayer graphene (TDBG) in proximity to WSe_2[36]. The structures are formed by stacking graphene layers with alternating twist angles as shown in Figure 2.10.

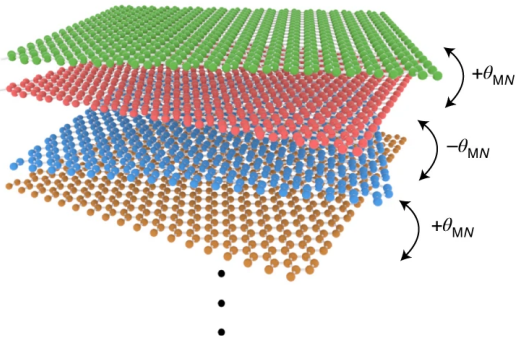

Figure 2.10: A twisted multilayer graphene structure with alternating twist angles. θ_{MN} is the magic angle corresponding to an N-layer structure. Extracted from: Robust superconductivity in magic-angle multilayer graphene family [27].

Independent of N, the moiré pattern created by stacking and twisting has a single periodicity determined by θ and the band structure can be calculated using the continuum Hamiltonian of TBG (given by equation 2.6), but extended to N-layers. In addition, the largest magic angle can be expressed in terms of its asymptotic limit as $N \to \infty$, as $\theta_N = \theta_\infty \cos\frac{\pi}{N+1}$, where $\theta_\infty = 2\theta_{N=2}$.

All the structures show a pair of flat bands at their magic angles, where each flat band has a four-fold band degeneracy and the density required to fill it completely from charge neutrality is $n_s = 8\theta^2/\sqrt{3}a_0^2$. It is therefore convenient to define ν, as $\nu = 4n/n_s$, $-4 < \nu < 4$ and use it to describe the carrier density n within the flat bands (measured from the charge neutrality point, CNP). This is the filling factor of the flat bands for MATBG and is defined as the number of carriers per moiré unit cell, ranging from -4 to 4. When ν is -4, 2, and 4 respectively, the flat band is empty, half-filled, and fully filled. Moreover, $\nu = \pm 1, \pm 2, \pm 3$ corresponds to one, two and three electrons (+) or holes (-) per moiré unit cell, respectively and $\nu = 0$ indicates the CNP.

Unlike MATBG, which has its flat bands isolated, the structures with $N > 2$ have them coexisting with other dispersive bands (see Figure 2.11) which strongly modify the electronic structures upon application of an out-of-plane displacement field. Consequently,

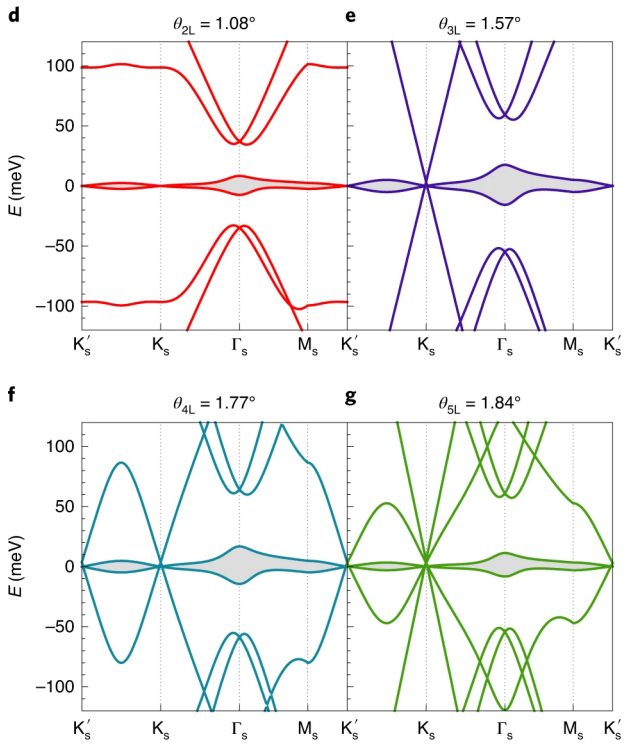

Figure 2.11: **d-g**, Calculated single-particle band structures of TBG, TTG, T4B, and T5B respectively near their magic angles and with zero electric displacement field. The shaded flat bands are shared by all systems. For all $N > 2$, the flat bands coexist with other dispersive bands. Extracted from: Robust superconductivity in magic-angle multilayer graphene family [27].

for $N > 2$, ν cannot be considered as the filling factor, since some of the charge carriers induced by the gate fill the dispersive bands. In fact, as N increases, the filling factor in the flat band is affected by the inhomogeneous distribution of carriers between the layers.

The question of why a monolayer of graphene does not exhibit superconductivity when several graphene structures do is expected. The answer lies in the vanishing of the DOS at the Dirac points as at low energies the DOS is linear in energy, and therefore it becomes zero at the Dirac points. On the other hand, in MATBG for instance, the DOS near the Dirac points is approximately three orders of magnitude than that of two uncoupled graphene sheets [9], hence, relatively weak or intermediate short-range repulsion interactions may not induce any phase transitions at low temperatures [13].

2.2 Mott-like insulators

We will devote this section to explaining a little about Mott-like insulators, as they are candidates for explaining the insulating states of MATBG at $\nu = \pm 2$ (see 4.1.1), and

are even considered to be the parent states of the superconducting phases observed near $\nu = \pm 2$. The theory is mainly based on ref. [37].

According to the band theory of metals, a half-filled and a full-filled valence band result in metallic conductivity and an insulator respectively, assuming that electron interactions are ignored. However, in 1937, Boer and Verwey reported that many transition metal oxides, such as NiO, are insulators, even though the d-band of these systems is partially filled by electrons [4]. Nevill Mott and Rudolf Peierls proposed electron correlations as an explanation: the insulating states are a consequence of the strong repulsive Coulomb interaction between electrons, which does not allow them to move to their nearest neighbouring sites, even if Pauli's exclusion principle is not violated.

One of the simplest theories explaining Mott-like insulators is the Mott-Hubbard picture, where the appearance of correlated insulators occurs when the condition $U/t \gg$ is satisfied, where U is the on-site Coulomb energy and t is the kinetic energy of the electron, which in the case of MATBG, is set by the bandwidth between the flat bands.

Chapter 3

Experimental methods

3.1 Experimental techniques used in the research

Some of the techniques used are:

1. **Scanning Tunnelling Microscopy, STM**: along with transport measurements, it can be used to identify the correlated insulators as the dips or pronounced minima in the plot of the differential conductance dI/dV as a function of carrier density. It also allows the direct visualization of the atomic structure, the local homogeneity of the twist angle, the domain walls, and the lattice disorder. How does it work? A metal tip is moved over a conductive sample without physical contact. A bias voltage is applied between the sample and the tip, allowing a current to flow between the two. The current is called a tunnelling current because the electrons have to overcome the distance, which acts as a barrier.

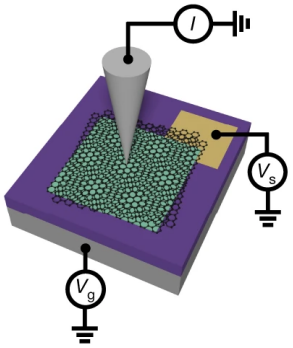

Figure 3.1: Example of a STM tip from which the tunnel current I is measured. A MATBG placed over a hBN/SiO_2/Si with a voltage V_s applied can also be seen. the V_g is used to tune the carrier density. Extracted from: Evidence for unconventional superconductivity in twisted bilayer graphene [32].

2. **Scanning Tunnelling Spectroscopy (STS)**: it measures the differential conductance, dI/dV, with respect to energy (commonly referred to as sample voltage, V_s) and is approximately proportional to the local electronic DOS at the tip position [1], therefore is used to localize the peaks in DOS. In STS, the bias voltage is the voltage difference between the tip and the sample as in STM. However, the main difference is that the bias voltage is modulated to vary the energy of the tunneling electrons. Since variations in the tunneling current can be related to changes in local charge density, it also allows studying the material's charge distribution.

3. **Landau-level spectroscopy**: is a technique in which electromagnetic radiation is applied to a 2D material in the presence of a perpendicular magnetic field. The aim of the radiation is to excite electrons between different Landau levels. By analyzing the absorption or emission of the radiation, electronic properties such as the effective mass of the charge carriers and the energy gaps between the Landau levels can be studied.

4. **Raman spectroscopy**: is a technique used to study the vibrational modes of atoms in a material and is based on the Raman scattering phenomenon, which involves the inelastic scattering of light by atoms. It can provide information about the crystal structure and chemical composition of the material.

5. **Andreev reflection spectroscopy**. Andreev reflection occurs at the interface between a normal metal (or any material with an excess of electrons) and a superconductor and is the process by which an electron from the normal metal entering the superconductor is reflected as a hole due to the presence of Cooper pairs. By measuring the energy and momentum of the reflected holes, the superconducting energy gap of the material can be determined[1]. It can also provide information about the nature of the superconductivity and the superconducting order parameter.

3.2 Sample preparation techniques

Figure 3.2 shows the basic structure of an encapsulated graphene device for electrical measurement. The device consists of graphene layers (the structure that will be studied); metallic gates and contacts, used as connection points to apply voltage, measure current through the graphene and perform transport or STS measurements; encapsulation layers, used to protect the graphene structure and contacts from environmental factors. These are typically flakes of hBN; a substrate, usually made of SiO_2, which provides mechanical support and electrical isolation for the entire device, and a top and bottom gate, used to modulate the total charge carrier density and interlayer potential difference. The bottom gate also helps to screen the charge impurities present in the substrate [10].

[1] Only the electrons with energy less than the superconducting gap are reflected

The device's fabrication consists of three steps [10]: 1) exfoliation, which consists of separating flakes of graphene, hBN, etc; 2) stacking and twist, and 3) clean room processing, where gates and electrical contacts to the heterostructure are made.

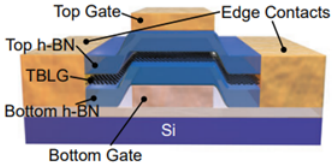

Figure 3.2: A typical TBG device. Extracted from: Study Of Electronic Correlation And Superconductivity In Twisted Graphene Superlattices [10].

An optical microscope and Raman spectroscopy can be used to characterize the thickness of the flake, and its quality can be characterized by performing atomic force microscopy (AFM), which allows imaging the microscopic wrinkles, cracks, holes, and other defects [10].

Precise control of the twist angle is essential to obtain a well-defined twisted structure. Two methods developed to achieve this are 'tear and stack' and 'cut and stack'.

'Tear and stack' technique

It consists of placing a graphene flake on SiO_2 and cutting it in two by pressing an hBN flake on one-half of it and lifting it up as graphene adheres strongly to hBN ((1) and (2) in Figure 3.3). Then, the other half left on SiO_2 is rotated by the desired twist angle before being picked up by the graphene-hBN stack ((4)-(6) in Figure 3.3). A disadvantage of this technique is the possible introduction of additional strain and defects into the twisted structure [10].

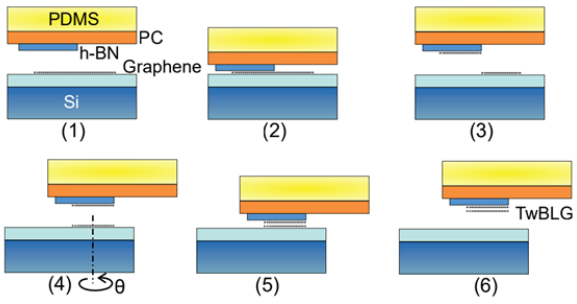

Figure 3.3: 'Tear and Stack' technique. Extracted from: Study Of Electronic Correlation And Superconductivity In Twisted Graphene Superlattices [10].

'Cut and stack' technique

It is a non-contacting method for cutting graphene or other thin flakes using focused laser beams. The success rate of cleanly ripping graphene can be more than 90% compared to 50% to 60% using 'tear and stack' [10], but it is more expensive and requires maintenance. To electrically contact the graphene structure, a method called 'edge contact' is widely used, where the metal electrodes are placed at the edges of the structure creating a pathway for electricity to flow.

One of the sample fabrication challenges is the twist inhomogeneity. 'Tear-and-stack' samples can have significant twist-angle inhomogeneity, which is considered to be introduced during sample fabrication [1]. This leads to inhomogeneity in the physical properties of the device as they vary sharply with moiré filling, which for a fixed electron density is inversely proportional to θ^2. However, inhomogeneity can be reduced by squeezing out bubbles and folds during sample fabrication, but at the cost of a less reliable overall twist-angle result. If TBG is naturally grown, the twist-angle can be homogeneous over a much larger area. As an alternative to tuning superconductivity with small twist angles, it has been shown experimentally that it can also be achieved by applying higher pressure to a device with a twist angle larger than the magic angle [42]. The more perfect the twist-angle control, the better the periodicity of the moiré pattern, and the richer the electronic phase diagram [1]. Moreover, twist angle inhomogeneity and other sources of disturbance can widen the flat bands and lead to very different behaviour near the magic angle in different TBG samples, making it difficult to provide reliable experimental constraints on a theoretical model [23].

In the case of MATTG, it is difficult to achieve the same twist angle between the top and middle layers (θ_{TM}) and between the middle and bottom layers (θ_{MB}) due to imperfect angel control and ubiquitous angle disorder, however, it has been found that the small angle difference does not affect the TTG device, in fact, the overall device twist angle measured corresponds to the average of the two angles, suggesting that the three layers behave as a single system resulting in a uniform device [15].

3.3 Measurements and analysis methods employed

TBG physics, especially near the magic angle, has a very small energy scale of < 10meV; therefore, it is necessary to cool it down to ultra-low temperatures [10], to carry out measurements, some of which are:

1. **Electrical transport measurements**: they mainly probe the electronic response of the charge carriers at the Fermi energy.

2. **Magneto-transport measurements**: they are experimental techniques used to study how the electrical properties of a material change in response to an applied magnetic field. They can also be used to identify spontaneously broken lattice rotational symmetry in the normal and superconducting phases.

3. **Density of states (DOS) measurements**: the DOS is studied by plotting dI/dV against sample voltage (as dI/dV is proportional to DOS), hence by using STS. It is also measured to identify superconducting coherence peaks.

4. **Voltage-current (V-I) and phase diagram**: these measurements are used to study the different phases of the material, such as superconductivity and correlated insulators.

5. **Extraction of the Berezinskii-Kosterlitz-Thouless transition temperature, $T_{\mathbf{BKT}}$**: the T_{BKT} describes a phase transition occurring in two-dimensional systems. Below this temperature, pair of particles starts to form and interact in a way that prevents them from being too far apart from each other. It can be found experimentally from the $I-V$ curves at different temperatures on a log-log scale, where it can be seen how the curves change from high-power polynomial to linear behaviour (characteristic of a metallic phase) in the low current and voltage range. The temperature is extracted from the line where $V \propto I^3$.

6. **The Ginzburg-Landau (GL) coherence length ξ_{GL}**. ξ_{GL} is a parameter used in the Ginzburg-Landau theory of superconductivity. It characterizes the spatial extent over which the superconducting order parameter decays from its maximum value to zero. It can be extracted from the theory for a 2D superconductor that establishes the following relation: $B_c = (\Phi_0/2\pi\xi_{GL}^2)\left(1-\frac{T}{T_C}\right)$, where B_c is the critical magnetic field, Φ_0 is the superconducting flux quantum and T_c is the critical temperature, which is sometimes taken to be the same as the value of T_{BKT}.

Chapter 4

Results and discussion

This section examines the experimental findings on superconductivity in twisted bilayer and twisted trilayer graphene from a theoretical perspective. Additionally, the nature of superconductivity, the potential superconducting mechanism, and unanswered concerns for MATBG, as well as the band structure and proof of unconventional superconductivity for MATTG, are examined. Finally, the superconductivity discovered in other graphene structures with $N > 3$ is briefly studied and contrasted with that of MATBG and MATTG.

4.1 Twisted Bilayer Graphene

4.1.1 Experimental results related to superconductivity in MATBG

The discovery that MATBG exhibits intriguing quantum states such as superconductivity and correlated insulators was made by physicists at the Massachusetts Institute of Technology (MIT) and Harvard University. The MIT group, led by Spanish physicist Pablo Jarillo-Herrero, started working with rotated graphene bilayers in 2010, and in 2016, they experimentally discovered that they exhibit interesting changes in their electronic structure at a rotation angle of 1.8°, which led them to study the system at smaller angles. In 2017, they managed to produce systems with rotation angles in the $1 - 1.2°$ range, discovering unexpected phenomena that were published in a paper in the journal Nature on March 5, 2018 [9]. We now present the main experimental results related to superconductivity in MATBG.

It exhibits flat low-energy bands which give rise to a high DOS

The flattening of the low-energy bands of TBG near the first magic angle was theoretically predicted by R. Bistritzer and A. MacDonald (2011) [3] (see 2.1.2) and it has been experimentally confirmed by Cao, Y. *et al.* (2018) [7]. The presence of the flat bands in their experiment was indicated by the large decrease in the Fermi velocity of the electrons, a characteristic expected for flat bands. As explained in ref. [10], the flatness of these bands can be demonstrated by measuring the Fermi velocity near the Dirac points using two methods. One of them is to measure the effective mass in the flat bands by means of quantum oscillations, which is done by fitting the amplitudes of the oscillations at different densities according to the Lifshitz-Kosevich formula. Using this method, a velocity of $4 \cdot 10^4$m/s has been found in the vicinity of the CNP [10]. The second method is to measure the quantum capacitance of MATBG near the Dirac point, which follows the expression $C_q = e^2 \frac{2\sqrt{2}}{\sqrt{\pi}\hbar v_F} \sqrt{|n|}$. By comparison with the experimental data, a velocity of $v_F = 1.5 \cdot 10^5$ is needed for a good fit [10].

Superconductivity can be tuned

It has be shown in many experiments that superconductivity can be achieved at a precise "magic angle", $\theta_M \approx 1.1°$ [9], [7], [23] and at a twist angle larger than 1.1° by varying the interlayer spacing with hydrostatic pressure [42]. One of the advantages of tuning superconductivity with pressure is that it can eliminate the need for precise angular tuning and potentially reduce the effects of structural inhomogeneity of the moiré pattern; in addition, working with a higher twist angle may be a way to increase the energy scale of the superconductor[1] [42].

Discovery of correlated insulating states

Correlated insulating states were first discovered close to half-filling of the flat bands ($\nu = \pm 2$) [9]. However, observations made in a MATBG device with improved twist-angle homogeneity showed correlated insulating states at all integer fillings: $\nu = 0, \pm 1, \pm 2, \pm 3, \pm 4$ [24]. They were identified as strong resistance peaks in a plot of the 4-terminal longitudinal resistance $R_{xx}(n)$ as a function of carrier density for different values of perpendicular magnetic field and at a base temperature of 16mK (see Figure 4.1). The insulating states at $\nu = \pm 1, \pm 2, \pm 3$ are correlated insulators (or correlated states) because their occurrence can only be explained by strong interactions between the electrons. Specifically, they emerge as a consequence of the localization of the electrons in the flat band, which leads to a high density of states and causes strong repulsion between them. Furthermore,

[1] The energy scale of a superconductor refers to the characteristic energy values associated with its superconducting behavior, such as the superconducting gap.

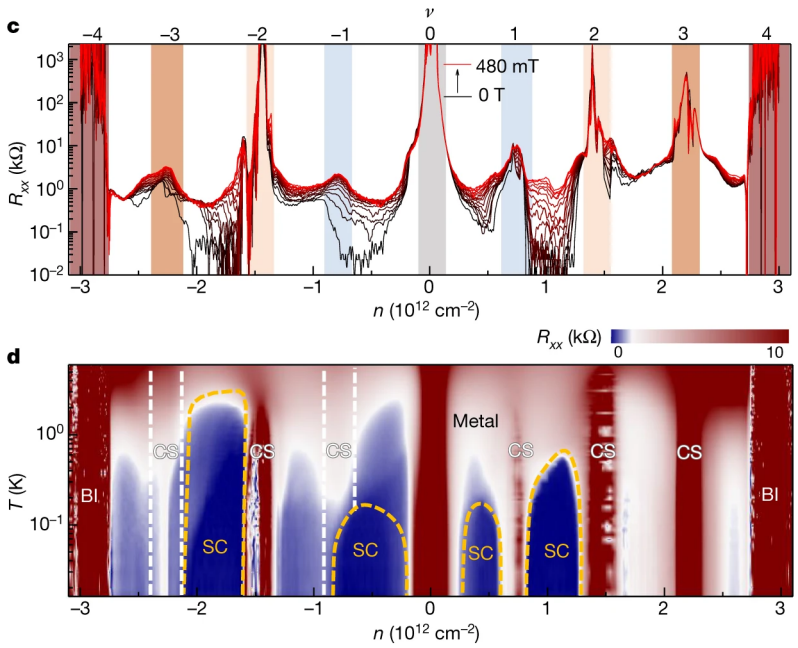

Figure 4.1: Top: $R_{xx}(n)$ as a function of carrier density n for different perpendicular magnetic fields from 0T (black curve) to 480mT (red curve) and at a base temperature of 16mK for a device with $\theta = 1.1°$. Bottom: Color plot of R_{xx} vs. n and T. Several phases can be seen such as metal, band insulator (BI), correlated state (CS), and superconducting state (SC) for the same device. The dashed lines indicate the boundary of the phases. Extracted from: Superconductors, orbital magnets and correlated states in magic-angle bilayer graphene [24].

it seems that they are associated with the magic angle, as at other angles, such as 0.8° and 1.3°, the system conducts very well [16]. This association has been confirmed by M. Yankowitz *et al.* (2019), who observed weak correlated insulators at $\pm n_s/2$ and around $\pm 3n_s/4$ at zero pressure, and no evidence of superconductivity in a 1.27° twist angle device [42]. While the insulating states at $\nu = \pm 4$ correspond to the band gaps above and below the flat bands (the already mentioned superlattice gaps).

The CSs at $\nu = \pm 2$ are proposed to be Mott-like insulators, as they appear to follow the Mott-Hubbard model by making simplistic estimates [7]. This is also supported by the Shubnikov–de Haas oscillation frequency f_{SdH} [7]. Nevertheless, other candidates have been proposed to describe them, such as charge density waves[2], Wigner crystals[3], and isospin ferromagnetic band insulators [42]. The observation pointing to Wigner crystals is that the insulating states are found to be very sensitive to external magnetic fields, which is not typical of Mott systems but, according to experiments, is highly relevant in

[2]A charge-density-wave (CDW) phase is a macroscopic quantum state consisting of a periodic modulation of the electronic charge density accompanied by a periodic distortion of the atomic lattice. Unconventional forms of superconductivity frequently emerge from this phase [2].

[3]The Wigner crystal is a state that occurs in the limit where the ratio of the Coulomb interaction to the kinetic energy is much greater than unity [34]. In this state, the electrons settle at the bottom of the respective potential 'dimples' in which they reside [6], essentially localizing into a crystalline structure and spontaneously breaking translational symmetry [34].

the case of Wigner crystals [6].

Since typical graphene is a very good conductor of electricity and has no energy gap, the insulating behavior is quite remarkable.

Emergence of superconducting domes near the correlated insulating states

Superconducting states are observed upon doping slightly away from the densities where the correlated insulating states appear (see figure 4.1). The superconducting domes in Figure 4.1 are identified by observing that the resistivity of the device measured at 16mK drops to zero at those regions, and can be returned to its original value with the application of a small perpendicular magnetic field, which is expected as superconductivity can be suppressed by the application of a $B_{\perp}$. Moreover, their appearance over similar density ranges for both electron and hole carriers suggests a link between the mechanisms driving this phase for the two carrier types [42].

The fact that the superconducting domes are flanked by insulating states in Figure 4.1, suggests a coexistence between them and that they arise from the same mechanism. Since a similar coexistence is present in cuprates, this observation leads to the conjecture that superconductivity could be assisted by correlated insulators as explained for the former. Nevertheless, P. Stepanov *et al.* (2020) [35] questioned this idea and found that superconductivity in MATBG can exist independently of correlated insulating states, indicating that these phases are competing rather than sharing a common microscopic origin [35].

The experiment they performed consisted of placing a metallic graphite layer parallel to and closer than 10 nm to a MATBG device, both separated by insulating multilayers of hexagonal boron nitride (see figure 4.2). They took measurements in several TBG devices with twist angles close to the magic-angle. The design aimed to make the correlated insulating states disappear by suppressing U so that the $U/t \gg 1$ condition was not satisfied (2.2). U is suppressed by the small distance between the MATBG and the graphite layer (smaller than the moiré unit cell), which leads to the screening out of the Coulomb interactions within the first one. They observed that instead of becoming weaker, superconductivity remained strong even without the presence of correlated insulators, filling the space in the phase diagram left by the insulators and covering large areas of doping without any discontinuities (see Figure 4.3). The appearance of superconductivity in all devices was confirmed and the disappearance of correlated insulators due to disordered arrangement of atoms or impurities within the material was discarded. As shown in Figure 4.3, CIs are absent and SC persists in the devices with the smallest w and θ slightly higher than θ_M. On the other hand, the device with the largest w and $\theta = \theta_M$ shows superconductivity domes flanked by CIs. The emergence of SC without CIs is also supported by the observations of X. Liu *et al.* (2021) [23]. They screened the Coulomb interactions with

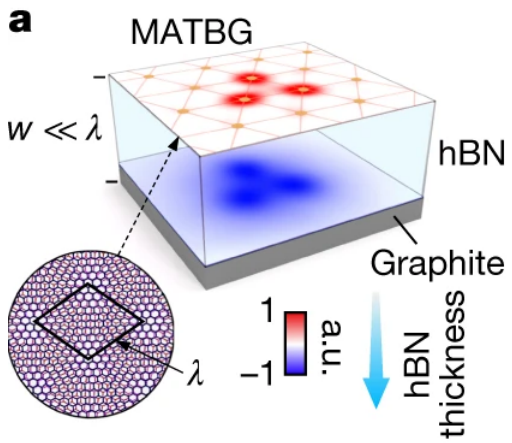

Figure 4.2: Design of the MATBG devices used in the experiment performed by P. Stepanov *et al.* (2020) to study the relationship between the superconducting and insulating states in MATBG. Wannier orbitals (red) in MATBG are screened by image charges on the graphite surface (blue). λ is the moiré lattice constant and w is the thickness of hBN. Extracted from: Untying the insulating and superconducting orders in magic-angle graphene [35].

a Bernal bilayer graphene (BLG) structure separated to a MATBG device of $\theta = 1.04°$ by a 3nm thickness of hBN. They studied the SC phase near $\nu = -2$ and found that it was more robust when the BLG was metallic, corresponding to stronger Coulomb screening (weaker CIs), compared to when the BLG was fully insulating, corresponding to minimal Coulomb screening (stronger CIs). However, unlike the first experiment, they could not completely suppress the CIs.

Although these results challenge the idea that MATBG is similar to cuprates, P. Stepanov *et al.* (2020) [35] found that the CIs reappeared in the presence of weak magnetic fields, indicating that they persist in the system, leaving the role of CIs in SC still unclear.

Nevertheless, the CIs may not be the only candidate precursors of superconductivity. E. Andrei and A. MacDonald (2020) [1] suggest that an observed nematic charge order[4], which is present only at hall filling and survives up to temperatures of about 35K and magnetic fields of ≈8T [17], may be an important precursor to the superconducting states that appear at lower temperatures.

Relatively high superconducting critical temperature

It has been found that the highest superconducting critical temperature occurs near $\nu = -2$ and is larger than 3K [24] which was previously found to be approximately 1.7K [9]. The critical temperature of superconducting cuprates, which are HTS, ranges

[4]Nematic charge order refers to the ordered arrangement of charged particles in a material. Here it results from the breaking of the rotational symmetry of the moiré cells.

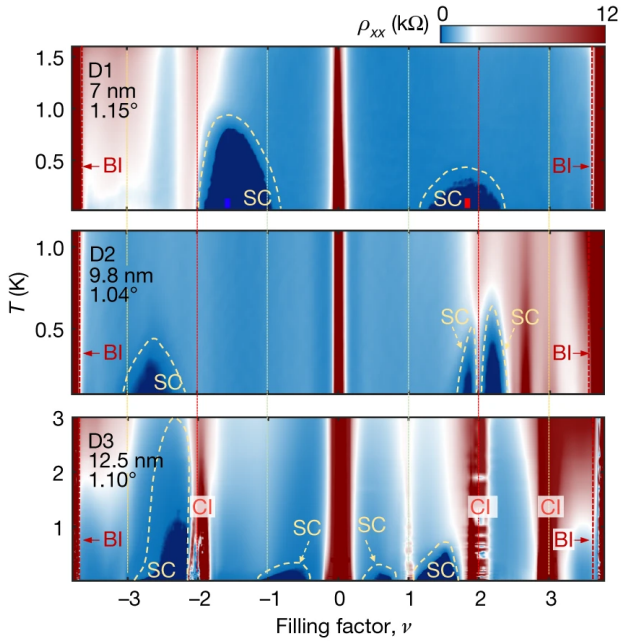

Figure 4.3: Resistivity ρ_{xx} as a function of ν and temperature T for the three screening MTABG devices: (D1) w≈ 7nm, $\theta \approx 1.15°$; (D2) w≈ 9.8nm, $\theta \approx 1.04°$ and (D3) w≈ 12.5nm, $\theta \approx 1.10°$. CI: correlated insulator; SC: superconductivity and BI: band insulator. Extracted from: Untying the insulating and superconducting orders in magic-angle graphene [35].

from 35K to 133K [39]. Compared to these temperatures, the critical temperature of MATBG is very low, which is an important parameter for applications, but not the most important parameter from a physical point of view. What physicists compare between superconductors is the charge density of the superconducting state. Therefore, what makes graphene special as a superconductor is its ability to superconduct at the temperature it does with so few electrons [16].

It has properties similar to those of high-temperature superconductors (HTS)

These properties are:

1. The superconducting domes seen in the phase diagram flank correlated insulators (see figure 4.1), similar to what is observed in the phase diagram of cuprates and pnictides shown in Figure 4.4, both HTS. However, in HTS there are typically two superconducting domes flanking an antiferromagnetic insulating state, but in ideal samples of MATBG insulating states can occur at all integer fillings, and superconducting domes can also appear close to them, even close to charge neutrality (see figure 4.1) [24].

2. The ratio of the critical temperature to the Fermi temperature, T_c/T_F, in MATBG is about 0.1 (when taking $T_C = 1.7$ K), exceeding the range at which BCS theory

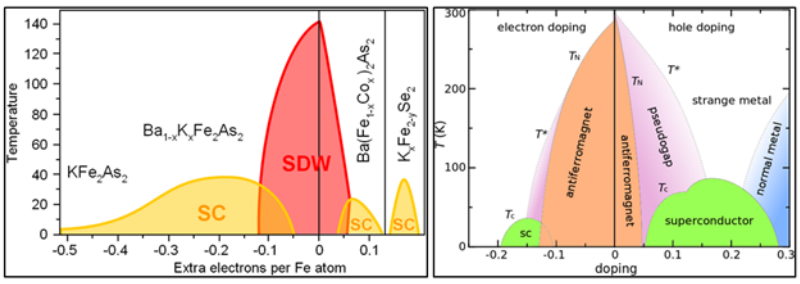

Figure 4.4: **Left**: Phase diagram of pnictides: two superconducting domes (yelow) flank a spin-density wave state (red). **Right**: Phase diagram of cuprates: two superconducting domes (green) flank an antiferromagnetic insulator phase (orange), a pseudogap and nematic phase (purple), a strange metal phase (white) and a normal metal (blue). Left picture was extracted from Elecronic band structure of ferro-pnictide superconductors from ARPES experiment [20] and created by Xantolus. Right picture was extracted from Cuprate superconductor [39] and created by Holger Motzkau.

can be used [1]. The value is actually similar to that of iron pnictides, cuprates, and FeSe(1L)/STO as shown in Figure 4.5.

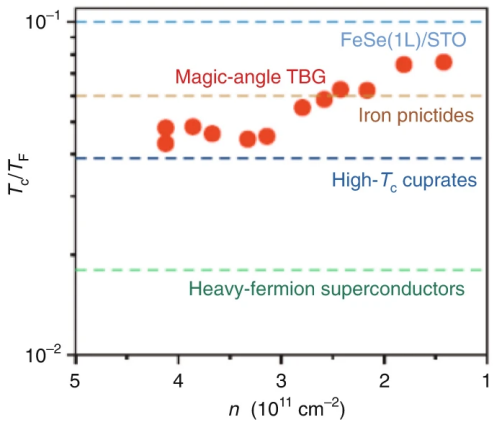

Figure 4.5: Ratio of the superconducting transition temperature to the Fermi temperature, T_c/T_F, as a function of doping n for MATBG (red circles) and other strongly correlated systems (marked by horizontal dashed lines). Extracted from: Graphene bilayers with a twist [1].

3. A pseudogap[5] opens at the Fermi energy (see Figure 4.6) when the flat bands are partially filled, giving way to a pseudogap phase, which is also found in cuprates and pnictides above the superconducting dome [18] (see Figure 4.4). In order to understand this strange phase, a quantum dimer model [31], but modified for a triangular lattice, was developed by J. Brunkert (2020) [5], which explains some of

[5]The pseudogap phase, which occurs in high-temperature superconductors, is an unconventional metallic phase with unusual properties. For example, it exhibits Fermi liquid-like transport, but an anomalously low carrier density [5].

the effects that occur in MATTBG in this phase and also predicts band splitting when a magnetic field is applied.

4. The appearance of a strange metal phase, which is common in strongly correlated superconductors such as cuprates (see Figure 4.4), pnictides, organic superconductors, and heavy fermions [1]. In a strange-metal phase, the electrical resistivity exhibits a linear or power-law dependence on temperature, indicating a breakdown of the usual metallic behavior. Resistivity measurements in MATBG doped within the flat band have shown a linear temperature dependence over a wide range of band filling, suggesting the existence of a strange metal phase above the superconducting domes (Y. Cao *et al.* (2020), R. Fernandes *et al.* (2019), cited in ref. [1]). However, this linear dependence may also be due to phonon scattering [1].

5. As in the case of HTS, MATBG also hosts broken symmetry states in the pseudogap and superconducting phase, such as nematic states (for example, the nematic charge order mentioned above), where the lattice rotational symmetry is broken but the lattice translational symmetry is not [17], [8]. These broken symmetry states can compete or coexist with the superconducting phase.

6. It has been found that on the underdoped side of the superconducting dome, close to $\nu = -2$, a normal-state anisotropic phase competes with superconductivity at low temperatures, lowering the value of T_c, similar to what has been seen in cuprates [8], [10].

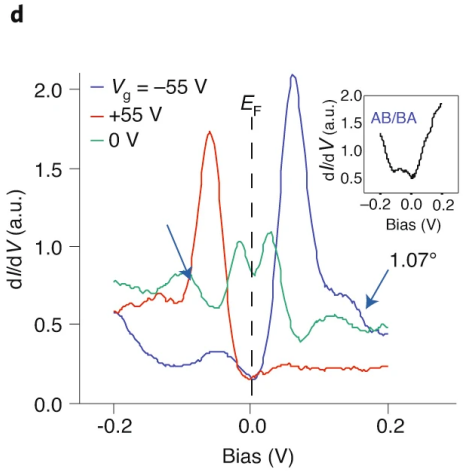

Figure 4.6: dI/dV spectra in the center of an AA region of MATBG with twist angle $\theta \approx 1.07°$ as a function of sample voltage. The red, blue, and green curves correspond when the flat bands are fully occupied ($V_g = 55$ V), empty ($V_g = -55$ V), and half filled ($V_g = 0$ V) respectively. The pseudogap can be seen in the green trace and it splits the DOS peak near the Dirac point (2.1.2). The Fermi level for all spectra is at zero bias voltage. Extracted from: Graphene bilayers with a twist [1].

4.1.2 Nematicity

The entire superconducting dome near $\nu = -2$ has been observed to exhibit nematicity[6], suggesting that nematicity is intrinsic to superconductivity and pointing to a possible unconventional pairing symmetry [10]. The nematicity of the superconducting dome is manifested in the response of the resistivity, critical current, and superconducting gap under the application of an in-plane magnetic field.

4.1.3 Is MATBG a conventional or unconventional superconductor?

The first evidence of possible unconventional superconductivity in MATBG is its similarity to cuprates through its phase diagram [9], [24]. Cuprates are known as high-temperature superconductors with a possible unconventional pairing mechanism (electron-electron interaction without the mediation of phonons) and are characterized by strong electron correlations leading to the formation of correlated insulators (as in MATBG). Besides this and some other similarities listed in 4.1.1, quantum oscillations in the longitudinal resistence of the material, indicating the presence of small Fermi surfaces near the correlated insulating states, have been observed in analogy to underdoped cuprates [9].

Another piece of evidence is the resemblance of the coherence peaks[7] to a nodal superconductor rather than an s-wave superconductor [26], whose pairing mechanism is usually well described by the BCS theory. Specifically, M. Oh *et al.* (2021) [26] observed that the tunneling spectra below T_c is inconsistent with the relationship for s-wave superconductors, but rather fits the plot corresponding to a nodal superconductor as it is shown in Figure 4.7, which is considered unconventional. Their experiment combined tunneling and Andreev reflection spectroscopy with a scanning tunneling microscope.

They also found that the tunneling gap persisted even when superconductivity was suppressed, suggesting that it originated from the pseudogap phase mentioned in 4.1.1, which is proposed to coexist and compete for dominance in certain regions of the phase diagram. In addition, the device studied showed contrasting behaviour between the energy scales describing tunneling and Andreev reflection, as has been observed in cuprates.

The observations challenging the alleged daughter-parent relationship between superconductivity and correlated insulators [11], [23], [32] point on the other hand to conventional superconductivity with electron-phonon coupling (supported by a number of theoretical models [41], [22], [12]) competing against Coulomb interactions to stabilize the supercon-

[6]Nematicity is a phenomenon where electrons in quantum materials can break rotational symmetry even when the underlying crystal lattice does not [8].

[7]Superconducting coherence peaks are sharp peaks in the DOS of a superconductor (i.e. in the tunneling spectra) and whose separation is associated with the superconducting gap.

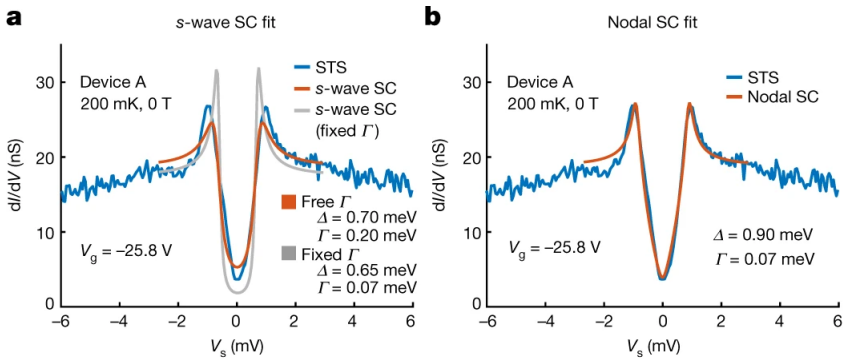

Figure 4.7: Left: Experimental Tunneling spectra (STS) of the superconducting phase near half-filling for a MATBG device with $\theta = 1.13°$ and $V_g = 25.8$V at 200mK and $B = 0$T (blue curve). In addition, Dynes-function using the model quasiparticle DOS for a nodeless s-wave superconductor with all free parameters (orange curve) and with fixed lifetime broadening parameter $\Gamma = 0.07$meV (grey curve). Right: Same as Left, except using the model quasiparticle DOS for a nodal superconductor. Extracted from: Evidence for unconventional superconductivity in twisted bilayer graphene [26].

ducting phase.

Y. Cao *et al.* (2018) [7] suggest that Coulomb interactions drive the formation of correlated insulators (which is also confirmed by the observation that screening produces the disappearance of the CIs, discussed in 4.1.1), whereas superconductivity arises from a more conventional mechanism, as the observation of resilience of superconductivity upon suppression of the insulating phase is more consistent with the two phases competing rather than being intimately coupled. [7].

However, S. Todadri (2020) [38] argues that although SC can be decoupled from the CIs, the superconductivity in the devices studied by Y. Saito *et al.* (2020) [32] and by P. Stepanov *et al.* (2020) [35] could be different from that found in older MATBG devices, like in [9], [24], [7] since in them superconductivity develops near half-filling from a normal state with a "small" Fermi surface, which is altered in the devices with no CIs.

E. Andrei *et al.* (2011) suggest that the observation that superconductivity is favoured over other states in the MATBG phase diagram when the electrical gates (used to vary ν) are moved closer to the bilayer may indicate that electron-electron interactions do not play the key role, shifting the balance towards phonon-mediated attraction.

Another observation that challenges the daughter-parent relationship between superconductivity and correlated insulators is that the two phases start at similar temperatures and that similar critical currents quench each phase to the normal-state resistance, suggesting that both share similar energy scales and are not directly linked as cause and effect [42].

The possible pairing mechanisms may also provide a clue to the nature of superconduc-

tivity.

4.1.4 Possible superconducting mechanism

Let us examine the possible pairing superconducting mechanisms in MATBG.

1. **Superconducting pairing due to the repulsive Coulomb interaction screened by electron-hole pairs, plasmons, and phonons** [11]. This superconducting pairing has been theoretically analyzed by T. Cea *et al.* (2021) using the Kohn-Luttinger formalism for the study of anisotropic superconductivity by repulsive interactions. Their results indicate the formation of Copper pairs and superconductivity in a significant range of twist angles ($\theta = 1.085°, 1.12°, 1.15°, 1.18°$) and fillings ($\nu = 0, \pm1, \pm2, \pm3, \pm4$). They found that screening by electron-hole pairs and plasmons leads to anisotropic superconductivity with a $T_c \sim 10^{-3} - 10^{-2}$K, which increases to $T_c \sim 1 - 10$K when phonons are considered. They also consider that Umklapp processes [8] play a crucial role in the formation of Cooper pairs.

2. **Phonon-mediated superconductivity**. In this mechanism, the phonons create an attraction between the electrons to form Cooper pairs. Theoretical studies [41], [22], [12] have shown that it could be a strong candidate, as it can explain the critical temperatures obtained experimentally, the robust superconductivity observed in MATBG and MATTG and the weak and almost absent superconductivity reported for twisted double bilayer graphene (TDBG) and twisted monolayer bilayer graphene (TMBG) at their respective magic angles.

   In the model proposed by F. Wu *et al.* (2018) [41], phonons form Cooper pairs in both ways: s-wave pairing and d-wave pairing, the former being more favourable before the inclusion of Columb repulsion. Moreover, the amplitude of the wave function describing the Cooper pair varies spatially with the Moiré period and is identical in the two layers for s-wave symmetry but has the opposite sign for d-wave symmetry. In their calculations, L. Biao *et al.* (2019) [22] predict that superconductivity can also be observed in TBG at many other angles and higher electron densities in higher moiré bands.

   However, the question of whether or not all flat-band states in graphene moiré superlattices exhibit such strong electron-phonon coupling remains unanswered [12].

   According to experimental data from X. Liu *et al.* (2021) [23], superconductivity at $\nu = -2$ becomes more robust with increasing Coulomb screening, which is consistent with electron-phonon coupling competing with Coulomb interactions to stabilize the superconducting phase.

[8] In an Umklapp process, an electron scatters a phonon in such a way that its momentum changes by a reciprocal lattice vector.

Finally, if this mechanism were present, X. Lu *et al.* (2019) [24] propose that it would be enhanced by the high density of states and electron correlation effects suggested by the anomalous nature of superconductivity at record low carrier densities.

3. **Collective excitations of strongly coupled electrons**. In this context, "collective excitations" refer to the coherent motion or behavior of multiple electrons together, rather than individual electron behavior. The role of correlated insulators in the emergence of superconductivity is still unclear, but Coulomb interactions and associated plasmonic effects are known to be very strong in graphene [33], hence G. Sharma *et al.* (2020) [33] propose that a superconducting state can be achieved by collective electronic modes near the magic angle in TBG. They use the Migdal-Eliashberg framework on a one-parameter effective lattice model for TBG and predict the presence of an asymmetric superconducting dome around $n = 10^{12}\text{cm}^{-2}$ and a $T_c = \mathcal{O}(10K)$, both in good agreement with recent experimental data.

   The idea that superconductivity in MATBG originates from electron correlations is also supported by the large ratio $T_C/T_F = 0.1$ when taking $T_F = 1.7$ K [9].

Open questions

Although research on MATBG has become a trend in the scientific community in recent years, there is still a lot of work to be done to answer some questions, such as the source of the attractive interaction that pairs electrons in the flat bands over wide ranges of band filling, i.e., the pairing mechanism, the superconducting pairing symmetry, which superconducting mechanism admits nodal gap functions, what is the nature of the pseudogap regime, and what is the relationship between robust superconductivity and moderate screening.

4.2 Twisted Trilayer Graphene

Let us now turn our attention to twisted trilayer graphene, which, consists of three adjacent layers of graphene sequentially twisted by θ and $-\theta$, as mentioned in 2.1.2. This configuration can also be seen as three layers of graphene, with the top and bottom layers aligned and the middle layer twisted by θ. High-resolution scanning tunnelling microscopy and spectroscopy of MATTG has revealed a preference for A-tw-A[9] stacking in the moiré pattern [19].

[9] 'tw' denotes the middle twisted layer.

4.2.1 Band structure

As shown in Figure 2.11, the band structure of MATTG at low energy theoretically consists of a set of flat bands coexisting with gapless Dirac bands, which has been experimentally confirmed [28]. This is quite interesting because one would expect a more complex band structure, but it turns out to be just a combination of the band structure of a single-layer graphene and that of a MATBG, with the interlayer coupling strength enhanced by a factor of $\sqrt{2}$. When a perpendicular displacement field, D, is applied, the flat and Dirac bands hybridize (see Figure 4.8), breaking the mirror symmetry of the moiré lattice which prevented hybridization, allowing the control of the bandwidth and interaction strength in the flat bands.

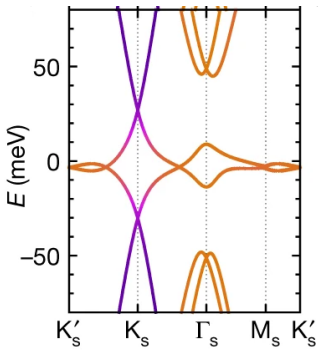

Figure 4.8: Calculated bandstructure of TTG with a twist angle $\theta = 1.57°$ ($\theta_{M3} \approx 1.6°$) at $D/\epsilon_0 = 0.2\text{Vnm}^{-1}$. Extracted from: Tunable strongly coupled superconductivity in magic-angle twisted trilayer graphene [28].

4.2.2 Experimental results related to superconductivity in MATTG

Resisitivity states

Resistivity states at $T = 70\text{mK}$ have been observed at $\nu = +1, \pm 2, +3, \pm 4$ regardless of D in a TTG device with $\theta = 1.57° \pm 0.02°$ [28]. In ref. [15], resistivity peaks are only found at $\nu = \pm 2, +1, +3$ at $T = 86\text{mK}$, which are modulated by D, and at $\nu = \pm 4$, the system has low resistivity.

Superconducting domes that can be tuned by varying D

Superconducting domes at $T = 70\text{mK}$ have been identified near $\nu = \pm 2$ at optimal displacement fields [28] as shown in Figure 4.9 in a TTG device with $\theta = 1.57° \pm 0.02°$. In ref. [15], where the TTG device has an average twist angle of $\theta \approx 1.56°$, superconductivity

is detected between $|\nu| = 2$ and $|\nu| = 3$ with a maximum T_c[10] of 2.1K, and in ref. [19], it is observed near $\nu = -2$.

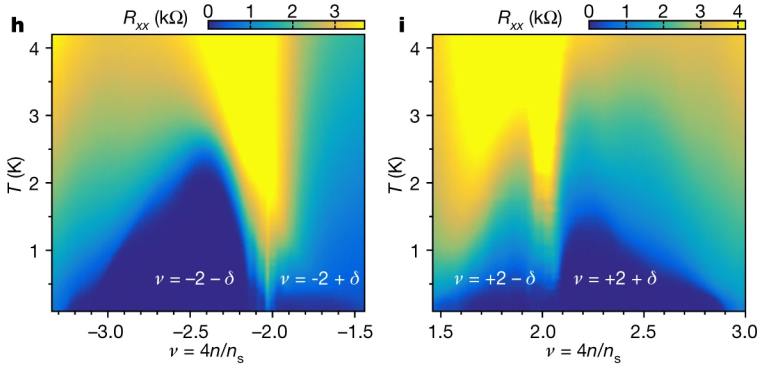

Figure 4.9: Longitudinal resistance $R_x x$ as a function of T and ν near $\nu = \mp 2$ when $D/\epsilon_0 = -0.44\text{Vnm}^{-1}$ and $D/\epsilon_0 = 0.74\text{Vnm}^{-1}$ respectively. $0 < \delta < 1$. Extracted from: Tunable strongly coupled superconductivity in magic-angle twisted trilayer graphene [28].

In Figure 4.9, the regions $\nu = -2 - \delta$ and $\nu = +2 + \delta$ with a critical temperature of about 2.9K and 1.4K respectively are considered robust superconducting regions[11]. The first one is identified by observing a sharp transition of the system from zero resistance up to a critical current of about 600nA to a resistive state. Such a sharp transition and the associated hysteresis are characteristic of robust superconductivity. The second one is identified by the observation of Josephson phase coherence near the boundary of the superconducting dome, even in the presence of a perpendicular magnetic field. To understand this better, let us break it down: a Josephson junction is formed by two superconducting materials separated by a thin insulating barrier (we assume that one of the materials is MATTG), but current can flow between them thanks to the tunneling effect. A magnetic field can affect the phase coherence between the wavefunctions of the Cooper pairs of each superconductor (in the coherent state, the phase difference is well defined and remains constant over time), possibly leading to a breakdown of the supercurrent and the loss of the properties associated with superconductivity. The fact that a coherence phase remains even in the presence of a magnetic field is therefore a signal that the phase of the wavefunction describing the Cooper pairs is not easily perturbed. On the other hand, $\nu = -2 + \delta$ and $\nu = +2 - \delta$ with $T_c < 1$K are identified as weaker superconducting regions. Furthermore, at small D (including zero), the superconductivity is restricted to the regions between $|\nu| = 2$ and $|\nu| = 3$. At large D, the phase diagram changes substantially and the superconductivity is bounded by VHSs in some regions, and extra branches of it strongly appear at $\nu = 2 - \delta$ [28].

In contrast, in ref. [15], the electron-side superconductivity is observed to be weaker and more affected by D, and the hole-side superconductivity is seen to persist for all D, with a

[10] In this experiment, T_C is defined as the temperature at which ρ falls to 10% of the normal state resistance.

[11] Robust superconductivity refers to the ability of a material to maintain its superconducting properties even in the presence of external perturbations or temperature changes.

width that first increases with D and starts to decrease at $D/\epsilon_0 \approx 0.4\text{Vnm}^{-1}$ (see Figure 4.10).

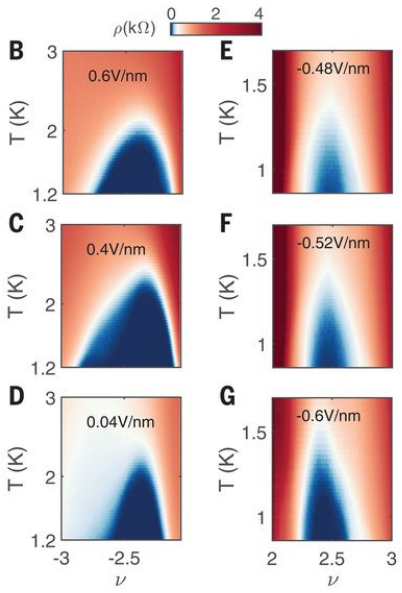

Figure 4.10: Domes-shaped superconducting regions in the $T - \nu$ plane at different D for $\nu < -2$ (**B** to **D**) and $\nu > 2$ (**E** to **G**). As it can be seen, the size and shape of the domes are tuned by D. Extracted from: Electric field–tunable superconductivity in alternating-twist magic-angle trilayer graphene [15].

In ref. [15], the dependence of T_c[12] on D is observed as follow: for the hole-side superconducting region, T_c first increases (**D** to **C**), reaching a maximum around $D/\epsilon_0 = 0.4\text{Vnm}^{-1}$, and then decreases (**C** to **B**). For the electron-side, T_c increases starting from $D/\epsilon_0 \approx 0.5\text{Vnm}^{-1}$ and then it starts to decrease at $D/\epsilon_0 = 0.62\text{Vnm}^{-1}$.

Observation of a strong-coupling nature of superconductivity

The strong-coupling nature of superconductivity in MATTG is highlighted by the high ratio $2\Delta/K_B T_c$ [19], which far exceeds the conventional BCS value of around 3.5.

Two superconducting regimes

Two distinct shapes in the tunnelling spectra are noted in ref. [19]: a U-shaped region and a V-shaped region (see Figure 4.11), suggesting two different superconducting regimes. They are further distinguished by transport measurements that reveal two different ξ_{GL} and by the magnetic field dependence of dI/dV: the field suppresses more efficiently the spectroscopic gap in the V-shaped regime compared with the U-shaped regime.

[12] T_c has been taken as the point at which $\rho = 10\%\rho_N$ and at $\nu = -2.3$ (hole-side) and $\nu = 2.45$ (electron-side).

The V-shaped tunnelling spectra resemble that of cuprates and can be well fit using the standard Dynes formula with a pairing order parameter that yields gapless nodal excitations[13]. On the other hand, the enhanced conductance suppression of the U-shaped spectra, points to the beginning of a fully gapped superconducting state.

Are the two superconducting regimes described by a BEC-BCS crossover or a BEC-BCS transition?

Here, when comparing a BCS and a BEC superconducting phase, the difference in both is that a BCS phase describes a superconductor for which the chemical potential μ intersects a flat band, independent of the pairing mechanism or the coupling strength. On the other hand, in a BEC phase, the chemical potential of the superconductor remains within the gap of the correlated insulator [19]. A BEC-BCS transition is different from a BEC-BCS crossover because in the latter the two regimes are fully gapped[14] and not topologically distinct.

In reference [28], the findings are that 1) MATTG has an extremely short zero temperature superconducting coherence length $\xi_{\mathrm{GL}(0)} \approx 12nm$ near the optimal point $(\nu_{\mathrm{opt}}, D_{\mathrm{opt}}/\epsilon_0) = (-2.4, -0.44\mathrm{Vnm}^{-1})$, which corresponds to the maximum T_{BKT}, and that 2) in the underdoped region of the superconducting dome, where the coherence length is limited by the interparticle distance, indicate that MATTG is a superconductor that can be tuned close to the BCS-BEC[15] crossover.

However, in ref. [19] a transition from a gapped BEC to a gapless BCS phase with a common nodal order parameter is proposed to explain the two observed superconducting regimes.

In MATBG, a BCS-BEC crossover is also suggested by the calculation of the coherence length, which is comparable to the interparticle distance, and by the value of the ratio T_c/T_{BEC}, which is estimated to be up to 0.37 [9].

4.2.3 Evidence for unconventional superconductivity in MATTG

We will now list some of the evidence, mainly provided by ref. [19], which points to unconventional superconductivity in MATTG. The TTG structure used was formed by alternately rotating three graphene layers by a twist angle $\theta = 1.51°$ and the study was

[13] Gapless nodal excitations here mean Cooper pairs that require little or no energy to break.

[14] A fully gapped superconductor is a superconductor that always has a non-zero superconducting gap and is well described by the BCS theory. However, not all superconductors are fully gapped. Some unconventional superconductors exhibit gapless or nodal excitations.

[15] BEC stands for Bose-Einstein Condensate.

carried out at 400mK using STM and focusing on the filling region where superconductivity had been observed.

1. **A pseudogap-like regime and coherence peaks that are suppressed with temperature and magnetic field, but persist well beyond the BCS limit**.

   The peaks around $V_{\text{bias}} = 0$V shown in Figure 4.11 resemble coherence peaks in superconductors and occur in the filling region where superconductivity has been observed [28], [15]. The possibility of fitting the V-shaped region to a nodal gap suggests unconventional superconductivity.

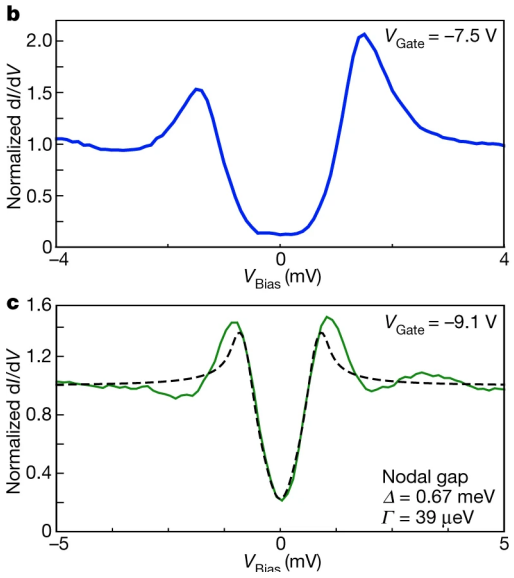

Figure 4.11: Differential conductance as a function of sample voltage. The top plot corresponds to $V_{\text{gate}} = -7.5$V, which belongs to a regime that follows a U-shape that doesn't adjust to a standard isotropic s-wave pairing order parameter fit. Meanwhile, the bottom plot represents a regime with a V-shape that can be fit to a nodal gap. Extracted from: Evidence for unconventional superconductivity in twisted trilayer graphene [19].

   The coherence peaks are observed to decrease gradually until 2-2.5K (close to the maximum critical temperature reported in transport) as T is increased. The hole-side peak completely disappears around 2.5K; however, the electron-side peak survives, but it is almost non-existent at $T^\star = 7$ K, where the differential conductance at $V_{\text{bias}} = 0$V still survives. This persistence beyond the disappearance of coherence peaks is typically interpreted as evidence of a pseudogap phase with a high transition temperature linked to $T^\star$, characteristic of unconventional superconductors.

2. **Tunnelling conductance profiles that are not adequately fit with an s-wave order parameter, but instead are compatible with gate-tuned transition from a gapped BEC to a gapless BCS phase with a common nodal order parameter**. See 4.2.2.

3. **Dip-hump structures in the differential conductance**. They are observed adjacent to the coherence peaks and persist over a broad doping range. Similar

dip–hump features are observed spectroscopically in conventional strongly coupled phonon superconductors, unconventional cuprate, iron-based, and heavy fermion superconductors. However, the ratio $\Omega/2\Delta$, where Ω is the bosonic-mode excitation energy and Δ is the superconducting gap, anticorrelates with Δ in the V-shaped regime, a trend observed in cuprates and iron-based compounds.

In addition, the observation of suppression of superconductivity upon reaching a VHS [28], [15] is taken as an indication that MATTG is unlikely to be consistent with the BCS theory, according to which the order parameter and related quantities (T_c, I_c, etc.) are generally positively correlated with the DOS.

4.3 Twisted Multilayer graphene

The superconductivity of MAT4G and MAT5G are briefly examined in this section, along with the distinctions and similarities between the superconductivity of MATBG and that of graphene structures with more than two layers. The results presented are mainly based on ref. [27].

Resistivity states

As compared to MATBG and MATTG, MAT4G and MAT5G are found to have significantly lower normal-state resistivity. The explanation proposed is the presence of extra highly dispersive Dirac bands, which provide parallel conducting channels. In addition, the resistivity states at $\nu = \pm 2$ are less resistive than those in MATTG and MATBG, and in some cases are even absent from the phase diagram, which is again attributed to the presence of additional Dirac bands at the Fermi level.

Observation of robust superconductivity

J. M. Park *et al.* (2022) [27] fabricated and measured several high-quality magic angle MAT4G and MAT5G devices, finding superconductivity in almost all of them, and it seems that as the number of graphene layers is increased, the superconductivity becomes more robust. In addition, similar to the MATTG, it can be tuned by means of a displacement field.

The fast switching behavior of the IV curves from a metallic to a superconducting phase and the broadening of the superconducting domes serve as evidence for robust superconductivity in MAT4G and MAT5G. Figure 4.12 shows that both devices exhibit superconductivity that begins about $\nu = \pm 1$ and reaches beyond $\nu = \pm 3$. In particular, MAT5G

exhibits superconductivity up to or even past $\nu = +4$. This finding suggests that adding more layers improves the phase space robustness of the superconductivity, especially in light of the fact that MATTG also had a broader dome than MATBG (compare Figures 4.1 and 4.9). However, one should remember that for $N > 2$, ν does not represent the filling factor of the flat bands.

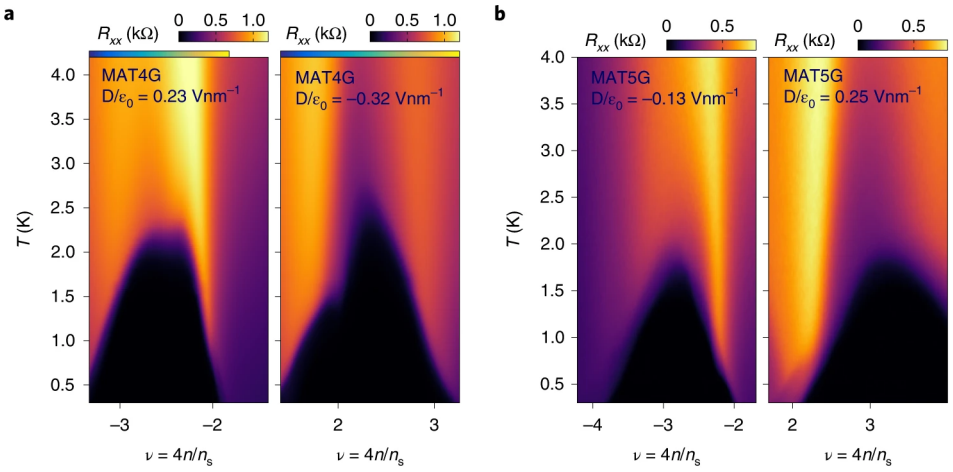

Figure 4.12: Resistance R_{xx} vs. moiré filling factor ν and T for a MAT4G and MAT5G devices with $\theta = 1.77°$ and $\theta = 1.76°$ respectively. Extracted from: Robust superconductivity in magic-angle multilayer graphene family [27].

Response to the application of in-plane magnetic fields

In MATTG, MAT4G, and MAT5G, the transition from superconductor to normal state does not depend on the direction of $B_{\parallel}$ and unlike MATBG, the former structures do not show any anisotropy of the $B_{c\parallel}$.

The Zeeman effect (caused by the application of a magnetic field) acting on the spin component of the Cooper pairs leads to a nominal Pauli paramagnetic limit, B_p, for conventional spin-singlet superconductors[16] with negligible spin-orbit interactions. MATTG has been found to violate the Pauli limit, as superconductivity persists up to fields ~ 3 times larger than the nominal Pauli limit. A similar violation has been observed in MAT4G and MAT5G, where the zero temperature critical fields, $B_{c\parallel}(0)$, exceed the Pauli limit by a factor of ~ 2 across all superconducting domes in all measured samples. On the other hand, in MATBG, $B_{c\parallel}(0)$ is around 1.1 T, which is higher than but close to $B_p \approx 0.93$T [9]. However, the suppression of superconductivity at fields of the order of B_p could also be due to an in-plane orbital effect, and as more layers are added, the in-plane orbital effects between the layers tend to cancel each other out.

Since the Pauli limit is violated in structures with $N > 2$ and possibly with N = 2, it is clear that their Cooper pairs cannot be spin singlets.

[16] B_p is estimated on the basis of the BCS theory and around it, Cooper pair breaking is expected.

Chapter 5

Conclusions

Writing this thesis was a bit of a challenge, but also extremely rewarding. It was inspiring to learn that the discovery of superconductivity in MATBG was born out of pure intellectual curiosity, showing us once again that asking new questions means real progress in science.

What can we conclude from this work? Firstly, since MATBG, MATTG, MAT4G, and MAT5G exhibit superconductivity and have flat bands at low energies, it is likely that these flat bands are crucial to the existence of superconductivity, and in the case of MATBG, the rotation symmetry may also be important as a nematic charge order is proposed to be a possible precursor to the superconducting states at half-filling. Secondly, the role of the correlated states in the appearance of superconductivity in MATBG is still unclear. However, I would say that the experimental observations tend to favor a competition between these two states rather than a parent-daughter relationship. Why? because we have seen that as N increases, the correlated states are less resistive at half-filling, while the observed superconductivity is more robust. And if the suggested explanation for the decrease in the resistance given in the literature is correct, they would not even share the same origin. Therefore, the study of structures with more layers might give a better insight into the claimed relationship. The layer limit that produces a 3-dimensional material (i.e. graphite), which is around 10 layers [29], could be an issue, though, which leads us to ask: Will the physics of 3D twisted multilayer be significantly different from that of 2D twisted multilayer graphene? Thirdly, the in-plane magnetic field response in the superconducting phase reveals a clear distinction between the $N = 2$ and $N > 2$-layer structures.

As for the nature of the superconductivity in the structures studied, the literature seems to point more to unconventional rather than conventional superconductivity, but clearly more research is needed. In the case of MATTG, it is still unknown whether the two superconducting regimes found correspond to a BEC-BCS crossover or a BEC-BCS transition.

In summary, Twisted Multilayer Graphene has proved to be an electrically tunable platform for the study of exotic quantum states, with its twist angle as a new degree of freedom, so its further study will continue, hopefully unraveling the nature and origin of its superconductivity. As for the potential applications, we need to be very patient, because it usually takes a long time to move from pure theoretical and experimental work to real applications. Fortunately, there is a lot of hype around graphene, and a lot of physicists are becoming more interested in graphene, including myself, so maybe we will not have to wait that long.

Conclusiones

Escribir esta tesis fue todo un reto, pero también extremadamente gratificante. Fue inspirador saber que el descubrimiento de la superconductividad en MATBG nació de pura curiosidad intelectual, lo que nos demuestra una vez más que plantearse nuevas preguntas supone un verdadero avance en la ciencia.

¿Qué podemos concluir de este trabajo? En primer lugar, dado que MATBG, MATTG, MAT4G y MAT5G presentan superconductividad y tienen bandas planas a bajas energías, es probable que ellas sean cruciales para la existencia de la primera y, en el caso de MATBG, la simetría de rotación también puede ser importante, ya que se ha propuesto que un orden de carga nemático sea un posible precursor de los estados superconductores a medio llenado. En segundo lugar, aún no está claro el papel de los estados correlacionados en la aparición de la superconductividad en MATBG. Sin embargo, yo diría que las observaciones experimentales tienden a favorecer una competencia entre estos dos estados más que una relación padre-hija. ¿Por qué? porque hemos visto que a medida que aumenta N, los estados correlacionados son menos resistivos a medio llenado, mientras que la superconductividad observada es más robusta. Y si la explicación sugerida para la disminución de la resistencia dada en la literatura es correcta, ni siquiera compartirían el mismo origen. Por lo tanto, el estudio de estructuras con más capas podría dar una idea más clara de la relación alegada. Sin embargo, el límite de capas que produce un material tridimensional (es decir, grafeno), que está en torno a las 10 capas [29], podría ser un problema, lo que nos lleva a preguntarnos: ¿Será la física del grafeno multicapa rotado en 3 dimensiones significativamente diferente de la de en 2 dimensiones? En tercer lugar, la respuesta del campo magnético paralelo a las estructuras en la fase superconductora revela una clara distinción entre los sistemas de capas con $N = 2$ y $N > 2$.

En cuanto a la naturaleza de la superconductividad en las estructuras estudiadas, la bibliografía parece apuntar más a una superconductividad no convencional que a una convencional, pero es evidente que se necesita más investigación. En el caso de MATTG, aún no está claro si los dos regímenes superconductores encontrados corresponden a un cruce BEC-BCS o a una transición BEC-BCS.

En resumen, el grafeno multicapa rotado ha demostrado ser una plataforma eléctricamente sintonizable para el estudio de estados cuánticos exóticos, con su ángulo de torsión como nuevo grado de libertad, por lo que su estudio continuará, quizá desentrañando la naturaleza y el origen de su superconductividad. En cuanto a las posibles aplicaciones, hay que tener mucha paciencia, pues normalmente se requiere mucho tiempo para pasar del trabajo puramente teórico y experimental a las aplicaciones reales. Afortunadamente, el grafeno está dando mucho de que hablar y muchos físicos, entre los que me incluyo, se están interesando cada vez más por él, así que quizá no tengamos que esperar tanto.

Bibliography

[1] E. Andrei and A. MacDonald. "Graphene bilayers with a twist". In: *Nature Materials* 19 (2020), pp. 1265–1275. DOI: 10.1038/s41563-020-00840-0. URL: https://doi.org/10.1038/s41563-020-00840-0.

[2] A. A. Balandin, S. V. Zaitsev-Zotov, and G. Grüner. "Charge-density-wave quantum materials and devices–New developments and future prospects". In: *Applied Physics Letters* 119 (2021), p. 170401. DOI: 10.1063/5.0074613. URL: https://doi.org/10.1063/5.0074613.

[3] R. Bistritzer and A. MacDonald. "Moiré bands in twisted double-layer graphene". In: *PNAS* 108.30 (May 2011), pp. 12233–12237. DOI: https://www.pnas.org/doi/full/10.1073/pnas.1108174108.

[4] J. H. de Boer and E. J. W. Verwey. "Semi-conductors with partially and with completely filled 3d-lattice bands". In: *Proceedings of the Physical Society* 49 (1937), p. 59. DOI: 10.1088/0959-5309/49/4S/307. URL: https://dx.doi.org/10.1088/0959-5309/49/4S/307.

[5] Julia Brunkert. "Effective theories for pseudogap metals". Master Thesis. Theoretical and Mathematical Physics (TMP): Ludwig-Maximilians-Universität München Technische Universität München, 2020.

[6] University of California San Diego. *Wigner Crystallization: A Brief Overview of the Theoretical and Experimental Development from its Inception to the Present*. Last accessed 27 August 2023. 2018. URL: https://courses.physics.ucsd.edu/2018/Fall/physics211a/topic/wigner.pdf.

[7] Y. Cao et al. "Correlated Insulator Behaviour at Half-Filling in Magic Angle Graphene Superlattices". In: *Nature* 556 (2018), pp. 80–84. DOI: https://www.nature.com/articles/nature26154.

[8] Y. Cao et al. "Nematicity and competing orders in superconducting magic-angle graphene". In: *Science* 372 (2021), pp. 264–271. DOI: 10.1126/science.abc2836. URL: https://www.science.org/doi/10.1126/science.abc2836.

[9] Y. Cao et al. "Unconventional superconductivity in magic-angle graphene superlattices". In: *Nature* 556 (2018), pp. 43–50. DOI: https://doi.org/10.1038/nature26160. URL: https://www.nature.com/articles/nature26160.

[10] Yuan Cao. "Study Of Electronic Correlation And Superconductivity In Twisted Graphene Superlattices". Doctoral Thesis. Department of Electrical Engineering and Computer Science: Massachusetts Institute of Technology, 2020.

[11] T. Cea and F. Guinea. "Coulomb interaction, phonons, and superconductivity in twisted bilayer graphene". In: *Proceedings of the National Academy of Sciences* 118.32 (2021), e2107874118. DOI: 10.1073/pnas.2107874118. URL: https://www.pnas.org/doi/abs/10.1073/pnas.2107874118.

[12] Y. W. Choi and H. J. Choi. "Dichotomy of Electron-Phonon Coupling in Graphene Moiré Flat Bands". In: *Physical Review Letters* 127.16 (Oct. 2021). DOI: 10.1103/physrevlett.127.167001. URL: https://doi.org/10.1103%2Fphysrevlett.127.167001.

[13] Y. Chu et al. "Superconductivity in twisted multilayer graphene: a smoking gun in recent condensed matter physics". In: *Chinese Physics B* 29.11 (2020), p. 117401. DOI: 10.1088/1674-1056/abbbea. URL: https://doi.org/10.1088%2F1674-1056%2Fabbbea.

[14] A. Geim and K. Novoselov. "The rise of graphene". In: *Nature Mater* 6 (2007), pp. 183–191. DOI: 10.1038/nmat1849. URL: https://doi.org/10.1038/nmat1849.

[15] Z. Hao et al. "Electric field–tunable superconductivity in alternating-twist magic-angle trilayer graphene". In: *Science* 371 (2021), pp. 1133–1138. DOI: 10.1126/science.abg0399. URL: https://doi.org/10.1038/s41586-021-03192-0.

[16] P. Jarillo-Herrero. *Conferencia: Grafeno de ángulo mágico: El "twist and shout" de los materiales cuánticos*. Last accessed 15 July 2023. 2020. URL: https://www.youtube.com/watch?v=tnFxblR4bSY.

[17] Y. Jiang et al. "Charge order and broken rotational symmetry in magic-angle twisted bilayer graphene". In: *Nature* 573 (2019), pp. 91–95. DOI: 10.1038/s41586-019-1460-4. URL: https://doi.org/10.1038/s41586-019-1460-4.

[18] B. Keimer et al. "From quantum matter to high-temperature superconductivity in copper oxides". In: *Nature* 518 (2015), pp. 179–186. DOI: 10.1038/nature14165. URL: https://doi.org/10.1038/nature14165.

[19] H. Kim et al. "Evidence for unconventional superconductivity in twisted trilayer graphene". In: *Nature* 606 (2022), pp. 494–500. DOI: 10.1038/s41586-022-04715-z. URL: https://doi.org/10.1038/s41586-022-04715-z.

[20] A. et al. Kordyuk. *Elecronic band structure of ferro-pnictide superconductors from ARPES experiment*. Last accessed 27 August 2023. 2011. URL: https://www.imp.kiev.ua/~kord/papers/FPS11/.

[21] L. D. Landau. "Zur Theorie der phasenumwandlungen II". In: *Phys. Z. Sowjetunion* 11 (1937), pp. 26–35.

[22] B. Lian, Z. Wang, and B. Andrei Bernevig. "Twisted Bilayer Graphene: A Phonon-Driven Superconductor". In: *Physical Review Letters* 122.25 (June 2019). DOI: 10.1103/physrevlett.122.257002. URL: https://doi.org/10.1103%2Fphysrevlett.122.257002.

[23] X. Liu et al. "Tuning electron correlation in magic-angle twisted bilayer graphene using Coulomb screening". In: *The American Association for the Advancement of Science* 371 (2021), pp. 1261–1265. DOI: https://www.science.org/doi/10.1126/science.abb8754.

[24] X. Lu et al. "Superconductors, orbital magnets and correlated states in magic-angle bilayer graphene". In: *Nature* 574 (2019), pp. 653–657. DOI: https://doi.org/10.1038/s41586-019-1695-0. URL: https://www.nature.com/articles/s41586-019-1695-0.

[25] K. S. Novoselov et al. "Electric Field Effect in Atomically Thin Carbon Films". In: *Science* 306 (2004), pp. 666–669. DOI: 10.1126/science.1102896. URL: https://www.science.org/doi/10.1126/science.1102896.

[26] M. Oh et al. "Evidence for unconventional superconductivity in twisted bilayer graphene". In: *Nature* 600 (2021), pp. 240–245. DOI: https://doi.org/10.1038/s41586-021-04121-x.

[27] J. M. Park et al. "Robust superconductivity in magic-angle multilayer graphene family". In: *Nature* 21 (2022), pp. 877–883. DOI: 10.1038/s41563-022-01287-1. URL: https://doi.org/10.1038/s41563-022-01287-1.

[28] J. M. Park et al. "Tunable strongly coupled superconductivity in magic-angle twisted trilayer graphene". In: *Nature* 590 (2021), pp. 249–255. DOI: 10.1038/s41586-021-03192-0. URL: https://doi.org/10.1038/s41586-021-03192-0.

[29] B. Partoens and F. M. Peeters. "From graphene to graphite: Electronic structure around the K point". In: *Phys. Rev. B* 74 (2006), p. 075404. DOI: 10.1103/PhysRevB.74.075404. URL: https://doi.org/10.1103/PhysRevB.74.075404.

[30] R. E. Peierls. "Quelques proprietes typiques des corpses solides". In: *Ann. I. H. Poincare* 5 (1935), pp. 177–222.

[31] M. Punk, A. Allais, and S. Sachdev. "A quantum dimer model for the pseudogap metal". In: *Proceedings of the National Academy of Sciences* 112 (2015), pp. 9552–9557. DOI: 10.1073/pnas.1512206112. URL: https://doi.org/10.1073%2Fpnas.1512206112.

[32] Y. Saito et al. "Independent superconductors and correlated insulators in twisted bilayer graphene". In: *Nature Physics* 16.9 (June 2020), pp. 926–930. DOI: 10.1038/s41567-020-0928-3. URL: https://doi.org/10.1038%2Fs41567-020-0928-3.

[33] G. Sharma et al. "Superconductivity from collective excitations in magic-angle twisted bilayer graphene". In: *Phys. Rev. Res.* 2 (May 2020). DOI: 10.1103/PhysRevResearch.2.022040. URL: https://journals.aps.org/prresearch/abstract/10.1103/PhysRevResearch.2.022040.

[34] T. Smoleński et al. "Signatures of Wigner crystal of electrons in a monolayer semiconductor". In: *Nature* 595 (2021), pp. 53–57. DOI: 10.1038/s41586-021-03590-4. URL: https://doi.org/10.1038/s41586-021-03590-4.

[35] P. Stepanov et al. "Untying the insulating and superconducting orders in magic-angle graphene". In: *Nature* 583 (2020), pp. 375–378. DOI: https://doi.org/10.1038/s41586-020-2459-6. URL: https://www.nature.com/articles/s41586-020-2459-6.

[36] R. Su et al. *Superconductivity in Twisted Double Bilayer Graphene Stabilized by WSe_2*. 2022. arXiv: 2211.16449 [cond-mat.supr-con].

[37] M. S. Suzuki. *Mott insulator and Hubbard model*. Last accessed 27 August 2023. 2019. URL: https://bingweb.binghamton.edu/~suzuki/SolidStatePhysics/20-2_Mott_insulator_and_Hubbard_model.pdf.

[38] S. Todadri. *What drives superconductivity in twisted bilayer graphene?* Journal Club for Condensed Matter Physics. 2020. URL: https://www.condmatjclub.org/?p=4208.

[39] Wikipedia. *Cuprate superconductor*. Last accessed 27 August 2023. 2023. URL: https://en.wikipedia.org/wiki/Cuprate_superconductor.

[40] Wikipedia. *Electronic properties of graphene*. Last accessed 01 Sepetember 2023. 2023. URL: https://en.wikipedia.org/wiki/Electronic_properties_of_graphene.

[41] F. Wu, A. MacDonald, and I. Martin. "Theory of Phonon-Mediated Superconductivity in Twisted Bilayer Graphene". In: *Physical Review Letters* 121.25 (Dec. 2018). DOI: 10.1103/physrevlett.121.257001. URL: https://doi.org/10.1103%2Fphysrevlett.121.257001.

[42] M. Yankowitz et al. "Tuning superconductivity in twisted bilayer graphene". In: *Science* 363 (2019), pp. 1059–1064. DOI: 10.1126/science.aav1910.